

Computing interface with quasiperiodicity

Duo Cao^a, Jie Shen^{a,1}, Jie Xu^{b,*,2}

^a Department of Mathematics, Purdue University, West Lafayette, IN, USA

^b LSEC & NCMIS, Institute of Computational Mathematics and Scientific/Engineering Computing (ICMSEC), Academy of Mathematics and Systems Science (AMSS), Chinese Academy of Sciences, Beijing, China



ARTICLE INFO

Article history:

Received 21 April 2020

Received in revised form 16 September 2020

Accepted 19 September 2020

Available online 24 September 2020

Keywords:

Interface

Quasicrystals

Dodecagonal phase

Gradient flows

Spectral methods

Scalar auxiliary variable (SAV)

ABSTRACT

We propose a method suitable for the computation of quasiperiodic interface, and apply it to simulate the interface between ordered phases in Lifschitz–Petrich model. The function space, initial and boundary conditions are carefully chosen so that it fixes the relative orientation and displacement, and we follow a gradient flow to let the interface find its optimal structure. The gradient flow is discretized by the scalar auxiliary variable (SAV) approach in time, and a spectral method in space using quasiperiodic Fourier series and generalized Jacobi polynomials. We use the method to study interface between striped, hexagonal and dodecagonal phases, especially when the interface is quasiperiodic. The numerical examples show that our method is efficient, accurate, and can successfully capture the interfacial structure.

© 2020 Elsevier Inc. All rights reserved.

1. Introduction

A modulated structure in space has long been viewed in history as a parallelepiped, typically cubic, unit cell occurring repeatedly in the space. A few obvious examples include lamellae, cylinder, and sphere structures. Some complex structures are also observed, such as gyroid structure. These structures have been found in various systems, including metals, colloids, block copolymer, liquid crystals, etc. [29,9,6]. Mathematically, they can be described by periodic functions in \mathbb{R}^3 . Despite their fancy appearance, we can always cut a unit cell from these structures. It was not until the 1980s that the first discovery of a 5-fold symmetry structure in a rapidly cooled Al-Mn alloy is reported in [30], which is recognized as quasicrystals years later. Since then, quasicrystals are observed in several other physical systems [25,45,13]. In quasicrystals, local morphology can be found repeatedly, but one can not find a unit cell. To describe quasicrystals, periodic functions are no longer appropriate, and one has to use quasiperiodic functions, which can be generated by the limitation of a periodic function in \mathbb{R}^n onto an \mathbb{R}^3 subspace. In this sense, a periodic structure can be regarded as special cases of quasicrystals. The most interesting fact about quasicrystals is that they can form symmetries, such as five-, eight-, ten- and twelve-fold rotations and icosahedral symmetries, which are not allowed by crystallographic space groups [24,7,1,2,16,18].

Studies of quasicrystals have been focused on the structures themselves. For the phase transitions involving quasicrystals, we currently know very little. Phase transitions can typically occur in two different ways: one phase loses stability and transforms into another as a whole; or two phases coexist for some time and the change mainly happens in the transition

* Corresponding author.

E-mail addresses: cao157@purdue.edu (D. Cao), shen7@purdue.edu (J. Shen), xujie@lsec.cc.ac.cn (J. Xu).

¹ The second author is partially supported by NSF DMS-1720442.

² The third author is partially supported by NSFC No. 11688101 and 12001524, NCMIS, and ICMSEC Director Funds.

zone. In the latter, the transition zone is understood as an interface between two structures. The driving force of the phase transitions comes from the interface where excess energy is stored. When modulated phases are involved, the morphology of interface becomes more complex, since the modulated phase possesses different intrinsic structures with different symmetries. For many materials consisting of modulated phases, the morphology of interface has a great effect on physical properties, such as elasticity and conductivity.

There are different viewpoints held on the interface. In many works, the interface is regarded as a transient state [8,27,20]. One could choose a finite domain, let two phases occupy two disjoint parts of the domain, and focus on the dynamics showing the movement of the interface. Studies of this kind are common for the interface between disordered phases such as water-vapor interface. The interface between modulated phases, however, usually has a long lifetime and is dependent on relative position and orientation. It is desirable to view the interface as a steady state under some constraints, so as to figure out the mechanism of connecting two modulated structures with different symmetries. From the above setting, it is difficult to control the relative position and orientation, and typically multiple structures are obtained that could interplay each other, making it difficult for us to identify the mechanism. Therefore, we choose the framework proposed in [41]. In that framework, the whole space is divided into three regions by two parallel planes. The two phases, with each phase being displaced or rotated, occupy the two on the sides, and a transition zone occurs in between. After posing the two phases as above, one then chooses the appropriate function space and boundary conditions that are able to describe both phases and constrain the relative position and orientation. In this function space, one could then let the system evolve to a local minimizer, typically under a gradient flow, to obtain the process for the interface to reach the optimal structure. Under this framework, we would understand the mechanism more clearly.

When quasicrystals are put into consideration, its intrinsic high-dimensional structure inevitably leads to numerical difficulty. It is already realized for bulk phases, as the numerical method has been discussed in [17] and applied to various systems [16,18,15]. One either needs to use Fourier series in a higher dimensional space, or approximate by the Fourier series in three-dimensional space with a carefully chosen period and a truncation at an extremely large number to adequately resolve the structure. The work [17] reveals that if the dimension and the truncation is considered altogether, it turns out that using higher dimensional approach has lower computational cost. This approach will also be adopted in the interface system.

For the interface system, we are facing further difficulties. Although the framework in [41] is clear, the numerical methods are not carefully designed previously. Only the special cases are examined where two phases are matched with common periodicity, and the numerical schemes adopted are naive. The first difficulty is that high-order spatial derivatives are involved, which is common in the models of quasicrystals. We use the Lifschitz–Petrich free energy [22], a model system that contains up to eighth-order spatial derivatives. The free energy requires conservation of mass, so the H^{-1} gradient flow will be studied. As a result, we need to solve a PDE with tenth-order spatial derivatives. To reach the accuracy that will not destruct the quasicrystalline structures, it is crucial to choose a robust spatial discretization. However, in the system for computing the interfacial structure, the Fourier series cannot be adopted directly, so that alternative methods need to be chosen. This will bring a second difficulty, that is, to specify suitable boundary conditions for numerical simulation. We need to displace and rotate its profile into a given position and orientation, then find the boundary conditions and set them for the interface system. These two steps are relatively easy for PDE, but become challenging for the discretized system. For the special cases where common periodicity exists, this problem could be evaded by using the same discretization for both the bulk profile and the interface system. However, this is no longer applicable for quasiperiodic interface. Since the spatial discretization will be different, when implementing the rotation and transformation between different discretization, we also need to guarantee reasonable accuracy that is able to keep the two phases on both sides. A third difficulty brought by the high-order spatial derivatives is for the time discretization of the gradient flow that requires energy stability. An ideal time discretization would combine energy stability, efficiency, accuracy and easy implementation.

Taking these difficulties into consideration, the finite difference and finite element methods that are used previously [42,40] are not suitable, because solving tenth-order PDEs by finite difference and finite element methods would be extremely complicated and suffers from prohibitively bad ill conditioning. Spectral-collocation method is also not appropriate as the quadratures involving derivatives at the boundary points are difficult to derive [14] and the conditioning is even worse than finite difference and finite element methods. We propose to use the spectral methods for spatial discretization, which are accurate enough to describe the quasiperiodic structures and are convenient to implement rotation and specify boundary conditions. Spectral-Galerkin methods have proved to be efficient and accurate for solving PDEs involving high order derivatives in simple geometries, which have been applied to the third-order KdV equation [32] and fourth-order equations [31,4] and even higher-order equations in [12,33]. Spectral-Galerkin methods embrace the advantage that the resulting linear system is sparse and well-conditioned, and in some cases fast direct solvers are available. Theoretical analysis and numerical results have shown the accuracy and efficiency for high-order PDEs [12,33]. For the interface system, we propose to use mixed Fourier series and generalized Jacobi polynomials (to enforce the non-periodic boundary conditions) as spatial discretization. As we have mentioned, quasicrystals need to be expressed by a function in a higher-dimensional space, in which the discretization is done. Thus, it is crucial to control the number of variables in each dimension. The spectral-Galerkin methods that we propose here are able to reach adequate accuracy with a relatively small number of variables in each dimension, greatly reducing the size of the discretized system, thereby improving significantly the efficiency.

For the time discretization, we use the SAV approach proposed recently for gradient flows [35,36]. The SAV approach leads to linearly implicit schemes with unconditional energy stability. Furthermore, the resulting linear system has constant coefficients that is easy to solve. This approach is extremely suitable when the free energy of the gradient flow has a dominant quadratic part, which is exactly the case for the Lifshitz–Petrich energy. Together with the spectral methods for spatial discretization, the linear system is block diagonal and can be solved efficiently. For the Lifshitz–Petrich energy, the convergence of the time discretization has actually been covered by the analysis in [34].

We apply the above numerical scheme for the quasicrystal interface, and examine some cases that are not dealt with previously. In particular, apart from the interface with a periodic structure, we focus on the quasiperiodic cases. These cases include the interface between periodic phases without common periodicity, or the interface involving quasicrystals. Some novel structures are presented. These examples clearly indicate the potential of our scheme to deal with a larger class of free energy functionals, such as free energy characterizing long-range pairwise interactions proposed for 3D icosahedral quasicrystals [2].

The rest of the paper is organized as follows. In Section 2, we describe the basic setting and discretization. We introduce the Lifshitz–Petrich free energy and the function space for quasicrystal solutions, followed by explaining the function space and boundary conditions for the interface system. In Section 3, we first discretize in time using the SAV scheme, followed by description of our spatial discretization, with Fourier series for two of the three directions, and generalized Jacobi polynomials for the other direction. Numerical results of interfacial structures will be presented in Section 4. Concluding remarks are given in Section 5.

2. The model

2.1. Lifshitz–Petrich model and quasicrystal solutions

The free energy of modulated phases, known as the Landau–Brazovskii model, is perhaps originated from Brazovskii [3], and has been studied in different contexts [37,10,19]. By modifying the Landau–Brazovskii model, some free energy functionals are proposed for quasicrystals [24,22,7]. We will consider the Lifshitz–Petrich (LP) free energy, which is proposed in [22] and has received much attention, given by

$$E[\phi(\mathbf{r}); \Omega] = \frac{1}{V(\Omega)} \int_{\Omega} \left\{ \frac{c}{2} [(\Delta + 1)(\Delta + q^2)\phi]^2 - \frac{\epsilon}{2}\phi^2 - \frac{\alpha}{3}\phi^3 + \frac{1}{4}\phi^4 \right\} d\mathbf{r}, \tag{1}$$

where $\Omega \subseteq \mathbb{R}^3$, $\mathbf{r} = (x, y, z)^t$, $V(\Omega)$ is the volume of Ω , and $q > 0$, $c > 0$, ϵ , α are phenomenological parameters. This free energy is simple while is able to describe many modulated phases including quasicrystals.

The bulk profile of a phase is obtained by minimizing the functional (1) when letting $\Omega \rightarrow \mathbb{R}^3$. If the phase is periodic with the unit cell Ω_0 , we can verify that

$$\lim_{\Omega \rightarrow \mathbb{R}^3} E[\phi(\mathbf{r}); \Omega] = E[\phi(\mathbf{r}); \Omega_0], \tag{2}$$

which is the energy density in the unit cell. On the other hand, the limit on the left-hand side is also suitable for quasicrystals. The free energy is characterized by the first term involving derivatives. We could comprehend its effect by choosing a single wave: let \mathbf{p} be a constant vector, and set $\phi(\mathbf{r}) = \cos(\mathbf{p} \cdot \mathbf{r})$ or $\sin(\mathbf{p} \cdot \mathbf{r})$ in (1), then the first term yields

$$\frac{c}{4}(1 - |\mathbf{p}|^2)^2(q^2 - |\mathbf{p}|^2)^2,$$

indicating that this term favors $|\mathbf{p}| = 1$ or $|\mathbf{p}| = q$. This term acts as a role of wavelength selection that suppresses the wavevectors far from the above two spherical surfaces.

For both periodic or quasiperiodic phases, the profile can be written in the following form:

$$\phi(\mathbf{r}) = \sum_{k_1, \dots, k_{d_0} \in \mathbb{Z}} \hat{\phi}_{k_1, \dots, k_{d_0}} \exp(i \sum_{j=1}^{d_0} k_j \mathbf{b}_j \cdot \mathbf{r}), \tag{3}$$

where i is the imaginary unit, and $\mathbf{b}_j (j = 1, \dots, d_0)$ are d_0 vectors in \mathbb{R}^3 that are linearly independent about the field of rational numbers \mathbb{Q} . In other words, if we have $\sum_{j=1}^{d_0} k_j \mathbf{b}_j = 0$ for some integers k_j , then we must have $k_j = 0$ for all j .

We define the d_0 -dimensional integer vector \mathbf{k} and the $3 \times d_0$ matrix B as

$$\mathbf{k} = (k_1, \dots, k_{d_0})^t, \quad B = (\mathbf{b}_1, \dots, \mathbf{b}_{d_0}). \tag{4}$$

The profile $\phi(\mathbf{r})$ can then be written as

$$\phi(\mathbf{r}) = \sum_{\mathbf{k} \in \mathbb{Z}^{d_0}} \hat{\phi}_{\mathbf{k}} \exp(i \mathbf{k}^t B^t \mathbf{r}). \tag{5}$$

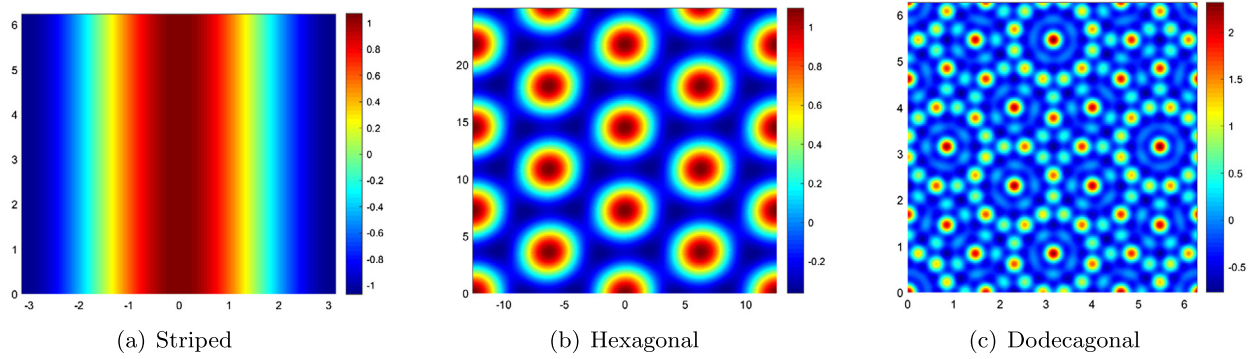


Fig. 1. Three patterns in the Lifschitz–Petrich model. (For interpretation of the colors in the figure(s), the reader is referred to the web version of this article.)

Taking this profile into the free energy (1), noticing the linear independence of \mathbf{b}_j and the equality

$$\lim_{\Omega \rightarrow \mathbb{R}^3} \frac{1}{V(\Omega)} \int_{\Omega} \exp(i\mathbf{p} \cdot \mathbf{r}) d\mathbf{r} = 0, \quad \mathbf{p} \neq \mathbf{0}, \tag{6}$$

we obtain

$$\begin{aligned} \lim_{\Omega \rightarrow \mathbb{R}^3} E[\phi(\mathbf{r}); \Omega] &= \frac{1}{2} \sum_{\mathbf{k} \in \mathbb{Z}^{d_0}} \left(c(1 - |B\mathbf{k}|^2)^2 (q^2 - |B\mathbf{k}|^2)^2 - \epsilon \right) \hat{\phi}_{\mathbf{k}} \hat{\phi}_{-\mathbf{k}} \\ &\quad - \frac{\alpha}{3} \sum_{\mathbf{k}_1 + \mathbf{k}_2 + \mathbf{k}_3 = \mathbf{0}} \hat{\phi}_{\mathbf{k}_1} \hat{\phi}_{\mathbf{k}_2} \hat{\phi}_{\mathbf{k}_3} + \frac{1}{4} \sum_{\mathbf{k}_1 + \mathbf{k}_2 + \mathbf{k}_3 + \mathbf{k}_4 = \mathbf{0}} \hat{\phi}_{\mathbf{k}_1} \hat{\phi}_{\mathbf{k}_2} \hat{\phi}_{\mathbf{k}_3} \hat{\phi}_{\mathbf{k}_4}. \end{aligned} \tag{7}$$

From the above expressions, we can see that the structure of a phase weighs heavily on the $3 \times d_0$ matrix B that is column full-rank on \mathbb{Q} . The matrix B determines whether the phase is periodic: if the column rank of B on \mathbb{R} is also d_0 (that implies $d_0 \leq 3$), then ϕ is periodic in \mathbb{R}^3 ; if the column rank of B on \mathbb{R} is strictly less than d_0 ($d_0 \geq 4$ belongs to this case), then ϕ is no longer periodic but quasiperiodic. In what follows, we write down the matrix B , under specific orientation, for three phases we will discuss in this paper: striped, hexagonal, and dodecagonal, which are drawn in Fig. 1. They all show modulation in at most two directions and are homogeneous in the third, which we can see from the matrix B . The former two phases are periodic, while the third is quasiperiodic. Rigorously speaking, the matrix B shall be optimized by minimizing (7). However, we choose to write down directly under the condition $|\mathbf{b}_j| = 1$ or $|\mathbf{b}_j| = q$, which is a suitably good approximation.

- Striped phase. Because we have two favored wavelengths, there are two cases:

$$B = \begin{pmatrix} 0 \\ 1 \\ 0 \end{pmatrix}, \quad B = \begin{pmatrix} 0 \\ q \\ 0 \end{pmatrix}. \tag{8}$$

The striped pattern is shown in Fig. 1 (a), where the two matrices give different widths of the stripe. Since the first and the third rows of B are zero, the phase profile ϕ does not depend on x and z , and only shows modulation in the y -direction.

- Hexagonal phase. Similar to the striped phase, we have two cases:

$$B = \begin{pmatrix} 1 & \frac{1}{2} \\ 0 & \frac{\sqrt{3}}{2} \\ 0 & 0 \end{pmatrix}, \quad B = \begin{pmatrix} q & \frac{q}{2} \\ 0 & \frac{\sqrt{3}q}{2} \\ 0 & 0 \end{pmatrix}. \tag{9}$$

The third row of B is zero, indicating that the profile ϕ is independent of z . The hexagonal pattern is drawn in Fig. 1 (b), where the two matrices give different distances between circles.

- Dodecagonal phase. We require $q = 2 \cos(\pi/12)$, and let

$$B = (\mathbf{b}_1, \mathbf{b}_2, \mathbf{b}_3, \mathbf{b}_4) = \begin{pmatrix} 1 & \frac{\sqrt{3}}{2} & \frac{1}{2} & 0 \\ 0 & \frac{1}{2} & \frac{\sqrt{3}}{2} & 1 \\ 0 & 0 & 0 & 0 \end{pmatrix}. \tag{10}$$

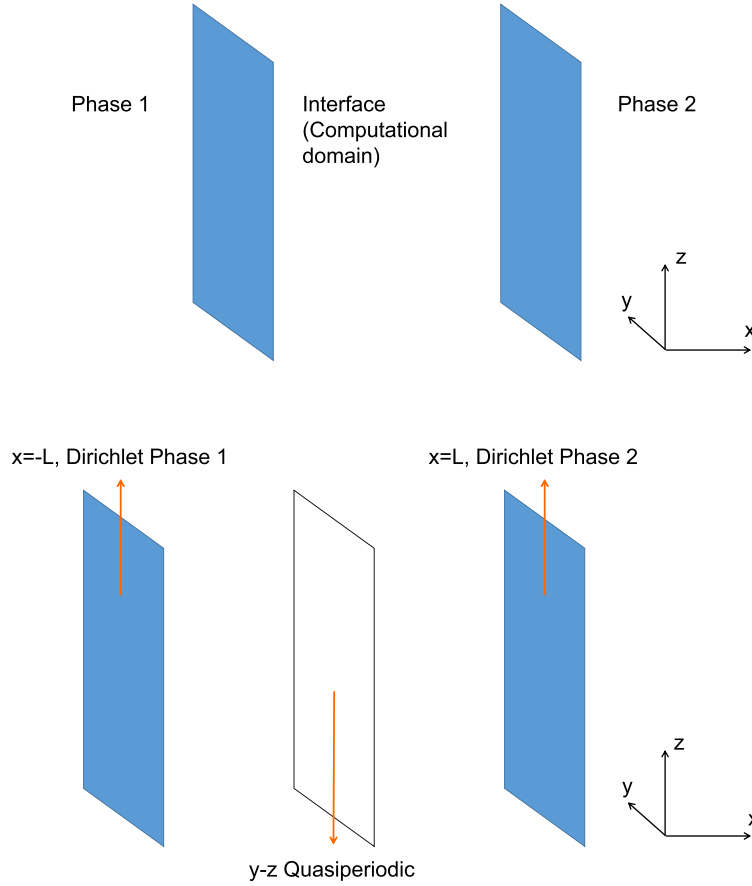


Fig. 2. Setting of the interface system.

Since the third row of B is zero, the dodecagonal phase has modulation in two directions. The value of q is chosen such that it equals to the length of the vector $\mathbf{b}_1 + \mathbf{b}_2$. We can verify that the four column vectors \mathbf{b}_j are linearly independent on \mathbb{Q} , by noting that 1 and $\sqrt{3}$ are linearly independent on \mathbb{Q} . Thus, we can see from B that the phase is quasiperiodic. The pattern is drawn in Fig. 1 (c), showing 12-fold symmetries that cannot be allowed in periodic phases.

2.2. General setting of the interface system

We divide the whole space into three regions by two parallel planes $x = -L$ and $x = L$ for some L . We assume that initially the phase 1 occupies the region $x \leq -L$, and the phase 2 occupies the region $x \geq L$ (see Fig. 2). Hence, the interface will form in the region $-L < x < L$. The final equilibrium state can be obtained by driving the gradient flow below to steady state,

$$\frac{\partial \phi}{\partial t} = \Delta \mu, \tag{11}$$

$$\mu = \frac{\delta E}{\delta \phi} = (\Delta + 1)^2 (\Delta + q^2)^2 \phi - \epsilon \phi - \alpha \phi^2 + \phi^3, \tag{12}$$

which is a tenth-order PDE for ϕ . In order for the gradient flow to describe the interface for certain relative position and orientation, we need to specify some conditions as described below.

First, we need to set the two phases in certain position and orientation. Suppose that the bulk profiles are given by ϕ_1 and ϕ_2 , where the B -matrices are B_1 with d_1 columns and B_2 with d_2 columns. We can express the two phase profiles after some rotation and displacement, denoted by ϕ_1^R and ϕ_2^R . For $T_s \in SO(3)$ and $\mathbf{p}_s \in \mathbb{R}^3$, the profile of the phase s ($s = 1, 2$) becomes

$$\phi_s^R(\mathbf{r}) = \phi_s(T_s \mathbf{r} + \mathbf{p}_s) = \sum_{\mathbf{k}_s \in \mathbb{Z}^{d_s}} \hat{\phi}_{s\mathbf{k}} \exp(i \mathbf{k}_s^t B_s^t (T_s \mathbf{r} + \mathbf{p}_s))$$

$$\begin{aligned}
 &= \sum_{\mathbf{k}_s \in \mathbb{Z}^{d_s}} \left(\hat{\phi}_{s\mathbf{k}_s} \exp(i\mathbf{k}_s^t B_s^t \mathbf{p}_s) \right) \exp\left(i\mathbf{k}_s^t (T_s^t B_s)^t \mathbf{r}\right) \\
 &= \sum_{\mathbf{k}_s \in \mathbb{Z}^{d_s}} \hat{\phi}_{s\mathbf{k}_s}^R \exp\left(i\mathbf{k}_s^t (T_s^t B_s)^t \mathbf{r}\right), \tag{13}
 \end{aligned}$$

where $\hat{\phi}_{s\mathbf{k}_s}^R = \hat{\phi}_{s\mathbf{k}_s} \exp(i\mathbf{k}_s^t B_s^t \mathbf{p}_s)$ and the superscript t means transpose.

Second, the information for $x \leq -L$ and $x \geq L$ can be translated into boundary conditions. Imagine that we choose a spherical domain with its center lying on the plane $x = -L$. In such a domain, the free energy shall be well-defined, so that certain continuity is required at $x = -L$. As a result of this requirement, the function value and the normal derivatives of ϕ on the boundary shall be identical to the bulk values, i.e.,

$$\frac{\partial^k}{\partial x^k} \phi(-L, \tilde{\mathbf{r}}) = \frac{\partial^k}{\partial x^k} \phi_1^R(-L, \tilde{\mathbf{r}}), \quad \frac{\partial^k}{\partial x^k} \phi(L, \tilde{\mathbf{r}}) = \frac{\partial^k}{\partial x^k} \phi_2^R(L, \tilde{\mathbf{r}}), \quad k = 0, 1, 2, 3, \tag{14}$$

where $\tilde{\mathbf{r}} = (y, z)^t$. Besides, the mass should be conserved in $-L < x < L$. So we impose the Neumann condition on μ ,

$$\frac{\partial \mu}{\partial \mathbf{n}} \Big|_{x=\pm L} = 0, \tag{15}$$

which implies the mass conservation.

Third, since we are studying a PDE on the whole y - z plane, we need to specify the function space in the y - z plane in which we solve the PDE. To this end, let us look back into the phase profile ϕ_s^R . For $s = 1, 2$, let us decompose the rotation matrix T_s as (T_{sx}, \tilde{T}_s) , where T_{sx} is the first column, and \tilde{T}_s is the second and third columns of T_s . Then, we write

$$\phi_s^R(x, \tilde{\mathbf{r}}) = \sum_{\mathbf{k}_s \in \mathbb{Z}^{n_s}} \hat{\phi}_{s\mathbf{k}_s}^R \exp\left(i\mathbf{k}_s^t (T_{sx}^t B_s)^t x\right) \exp\left(i\mathbf{k}_s^t (\tilde{T}_s^t B_s)^t \tilde{\mathbf{r}}\right), \tag{16}$$

and define $\tilde{B}_s = \tilde{T}_s^t B_s$ that is a $2 \times d_s$ matrix. For fixed x , $\phi_s^R(x, \tilde{\mathbf{r}})$ is in the function space

$$A_s = \left\{ \sum_{\mathbf{k}_s \in \mathbb{Z}^{d_s}} a_{\mathbf{k}_s}(x) \exp\left(i\mathbf{k}_s^t \tilde{B}_s^t \tilde{\mathbf{r}}\right) \right\}. \tag{17}$$

Now, let us consider the $2 \times (d_1 + d_2)$ matrix $(\tilde{B}_1, \tilde{B}_2)$. The column rank of this matrix on \mathbb{Q} is $d \leq d_1 + d_2$. Therefore, we can find a $2 \times d$ matrix B such that there exists an $d \times (d_1 + d_2)$ integer matrix Z satisfying

$$\tilde{B}Z = (\tilde{B}_1, \tilde{B}_2). \tag{18}$$

Define the function space

$$A = \left\{ \phi(\mathbf{r}) = \sum_{\mathbf{k} \in \mathbb{Z}^d} \phi_{\mathbf{k}}(x) \exp\left(i\mathbf{k}^t \tilde{B}^t \tilde{\mathbf{r}}\right) \right\}. \tag{19}$$

It can be verified that $A_1, A_2 \subseteq A$, since we have

$$\tilde{B}_1 \mathbf{k}_1 = (\tilde{B}_1, \tilde{B}_2) \begin{pmatrix} \mathbf{k}_1 \\ \mathbf{0} \end{pmatrix} = \tilde{B}Z \begin{pmatrix} \mathbf{k}_1 \\ \mathbf{0} \end{pmatrix}. \tag{20}$$

In this sense, the function space A is suitable for both phases. It is easy to verify that A is closed for linear combination, function multiplication and derivatives. So, if the initial condition of the gradient flow (11)–(12) is in A , the solution will remain in A .

It should be noted that the definition of the space A depends on \tilde{B}_1 and \tilde{B}_2 , which are determined by the bulk profile and the rotations T_1 and T_2 . In particular, even if the bulk phases are the same, for different rotations, the resulting function space will be different.

For a region \mathcal{D} in the y - z plane with the area $S(\mathcal{D})$, we define the inner product in $L^2((−L, L) \times \mathcal{D})$ by

$$(u, v) = \lim_{\mathcal{D} \rightarrow \mathbb{R}^2} \frac{1}{2S(\mathcal{D})L} \int_{(-L, L) \times \mathcal{D}} u(\mathbf{r})v(\mathbf{r}) \, d\mathbf{r} = \frac{1}{2L} \sum_{\mathbf{k} \in \mathbb{Z}^d} \int_{-L}^L u_{\mathbf{k}}(x)v_{-\mathbf{k}}(x) \, dx. \tag{21}$$

For the second equality above, we need to use the fact that \tilde{B} is column full-rank on \mathbb{Q} . The interfacial energy density is defined as

$$E_i = \lim_{\mathcal{D} \rightarrow \mathbb{R}^2} E[\phi(\mathbf{r}); -(L, L) \times \mathcal{D}], \tag{22}$$

for which we have the energy dissipation,

$$\frac{dE_i(\phi)}{dt} = \left(\frac{\delta E}{\delta \phi}, \frac{\partial \phi}{\partial t} \right) = -(\nabla \mu, \nabla \mu). \tag{23}$$

We can then express ϕ_s^R using the matrix \tilde{B} and the form given in (19). Denote by $\phi_{sk}^R(x)$ the coefficients (that take the place of $\phi_{\mathbf{k}}(x)$ in (19)), which are functions of x only. Taking ϕ_1^R as example, the coefficients are given by

$$\phi_{1\mathbf{k}}^R(x) = \sum_{\mathbf{k}_1} \hat{\phi}_{1\mathbf{k}_1}^R \exp(i\mathbf{k}_1^t B_1^t T_{1x} x), \quad \text{the sum is taken over } \mathbf{k} = Z \begin{pmatrix} \mathbf{k}_1^t \\ \mathbf{0} \end{pmatrix}. \tag{24}$$

We also write ϕ and μ in the form (19). The initial condition can be constructed by a simple mixing ansatz,

$$\phi_{\mathbf{k}}(x) = (1 - b(x))\phi_{1\mathbf{k}}^R(x) + b(x)\phi_{2\mathbf{k}}^R(x), \tag{25}$$

where $b(x)$ is a smooth monotone function satisfying $b(-L) = 0$ and $b(L) = 1$. A good approximation to $b(x)$ is

$$b(x) = \frac{1 - \tanh(\sigma x)}{2}, \tag{26}$$

with σ large.

To summarize, we need to find $\phi \in A$, which is the solution of the gradient flow (11)–(12) in $\Omega = (-L, L) \times \mathcal{D}$ with boundary conditions (14) and (15) and initial condition

$$\phi(\mathbf{r}, 0) = \sum_{\mathbf{k} \in \mathbb{Z}^d} [(1 - b(x))\phi_{1\mathbf{k}}^R(x) + b(x)\phi_{2\mathbf{k}}^R(x)] \exp(i\mathbf{k}^t \tilde{B}^t \tilde{\mathbf{r}}). \tag{27}$$

Remark. The boundary conditions and the function space A are consistent for a special case: if the two phases are identical, and the relative position and orientation is the same, there shall be no interface. In other words, this setting will not generate artificial interface.

The choice of L is case-dependent. It shall let the transition region between two phases not touch the boundary so that the Dirichlet boundary has little effect on the interfacial structure. Meanwhile, for efficiency L shall be as small as possible. A suitable choice shall balance these two requirements.

The Dirichlet boundary condition on $x = \pm L$ does not affect the well-posedness when $d \leq 2$ so that A consists of periodic functions (cf., for example, [38]). However, since the space of quasiperiodic function is related to a higher dimension, the well-posedness would depend on the decent understanding of such a function space, which, to the knowledge of the authors, is still unavailable.

3. The numerical method

To discretize the gradient flow (11)–(12), we first present the semi-discretized scheme in time using the SAV approach, followed by spatial discretization by generalized Jacobi polynomials.

3.1. Time discretization by the SAV approach

Let

$$E_1[\phi] = (F(\phi), 1), \quad F(\phi) = C_0 - \frac{\epsilon + \beta}{2} \phi^2 - \frac{\alpha}{3} \phi^3 + \frac{1}{4} \phi^4, \tag{28}$$

where $\beta > 0$ is a constant, C_0 is chosen such that $E_1(\phi) > 0$ for any ϕ . The polynomial $F(s)$ satisfies $\lim_{s \rightarrow \pm\infty} F(s) = +\infty$ and has at most three stationary points: zero, and $\frac{\alpha}{2} \pm \frac{1}{2} \sqrt{\alpha^2 + 4(\epsilon + \beta)}$ if they are real numbers. One could easily evaluate the minimum value of $F(s)$ and choose a C_0 such that the minimum value of $F(s)$ is not close to zero. In our simulations, it works well when C_0 is chosen such that $\min F(s) \approx 10^2$. An auxiliary variable $r(t) = \sqrt{E_1[\phi]}$ is introduced, so that the gradient flow is rewritten as

$$\begin{aligned} \frac{\partial \phi}{\partial t} &= \Delta \mu \\ \mu &= (c(\Delta + 1)^2(\Delta + q^2)^2 + \beta)\phi + \frac{r(t)}{\sqrt{E_1[\phi]}} F'(\phi) \\ r_t &= \lim_{\mathcal{D} \rightarrow \mathbb{R}^2} \frac{1}{2S(\mathcal{D})L} \int_{[-L, L] \times \mathcal{D}} \frac{F'(\phi)}{2\sqrt{E_1[\phi]}} \phi_t \, d\mathbf{r}. \end{aligned} \tag{29}$$

Taking the inner product with μ , $\partial\phi/\partial t$ on the first two equations, respectively, multiplying the third with $2r$ and adding three together, we arrive at the following energy dissipation law:

$$\frac{dE_i[\phi(t)]}{dt} = \frac{d}{dt} \left[\frac{c}{2} ((\Delta + 1)(\Delta + q^2)\phi, (\Delta + 1)(\Delta + q^2)) + \frac{\beta}{2} (\phi, \phi) + r^2 \right] = -(\nabla\mu, \nabla\mu). \tag{30}$$

For the interface system, we are more interested in the steady state, so we use the first-order scheme. Let Δt be a time step, and ϕ^n denote the numerical approximation to $\phi(\mathbf{r})$ at $t = t_n$. Then a first-order scheme in time for the above system can be constructed as follows:

$$\begin{aligned} \frac{\phi^{n+1} - \phi^n}{\Delta t} &= \Delta\mu^{n+1}, \\ \mu^{n+1} &= (c(\Delta + 1)^2(\Delta + q^2)^2 + \beta)\phi^{n+1} + \frac{r^{n+1}}{\sqrt{E_1[\phi^n]}} F'(\phi^n), \\ \frac{r^{n+1} - r^n}{\Delta t} &= \lim_{\mathcal{D} \rightarrow \mathbb{R}^2} \frac{1}{2LS(\mathcal{D})} \int_{[-L, L] \times \mathcal{D}} \frac{F'(\phi^n)}{2\sqrt{E_1[\phi^n]}} \frac{\phi^{n+1} - \phi^n}{\Delta t} d\mathbf{r}. \end{aligned} \tag{31}$$

The above scheme is linear but coupled. We will show below that it can be efficiently solved.

Theorem 1. *The scheme (31) is unconditionally energy stable in the sense that*

$$\begin{aligned} &\frac{1}{\Delta t} \left(\tilde{E}_i[\phi^{n+1}, r^{n+1}] - \tilde{E}_i[\phi^n, r^n] \right) \\ &+ \frac{1}{\Delta t} \left(\frac{c}{2} ((\Delta + 1)(\Delta + q^2)(\phi^{n+1} - \phi^n), (\Delta + 1)(\Delta + q^2)(\phi^{n+1} - \phi^n)) \right. \\ &\left. + \frac{\beta}{2} (\phi^{n+1} - \phi^n, \phi^{n+1} - \phi^n) + (r^{n+1} - r^n)^2 \right) = -(\nabla\mu^{n+1}, \nabla\mu^{n+1}), \end{aligned} \tag{32}$$

where the modified energy is defined as

$$\tilde{E}_i[\phi^n, r^n] = \frac{c}{2} ((\Delta + 1)(\Delta + q^2)\phi^n, (\Delta + 1)(\Delta + q^2)\phi^n) + \frac{\beta}{2} (\phi^n, \phi^n) + (r^n)^2. \tag{33}$$

Proof. Taking the inner product of the first two equations with μ^{n+1} , $\phi^{n+1} - \phi^n$, respectively, multiplying the third with $2r^{n+1}$, noticing the equality $(b - a, 2b) = b^2 - a^2 + (b - a)^2$, we obtain (32). \square

Adaptive time stepping. In our interface system, the energy curve about the time descends drastically at the early stage but becomes flat afterwards as it approaches the steady state. Therefore, we adopt an adaptive time stepping method, using small time steps initially and large time steps when the energy is decreasing slowly. We choose the empirical time step updating strategy suggested in [28] and successfully applied in various systems [46,43,44,5],

$$\Delta t_{n+1} = \max \left(\Delta t_{\min}, \frac{\Delta t_{\max}}{\sqrt{1 + \eta |E^{n+1}(t) - E^n(t)|^2 / \Delta t_n^2}} \right), \tag{34}$$

where Δt_{\min} , Δt_{\max} are predetermined minimum and maximum time steps and η is a suitable parameter, taken as $\eta = 1000$ in our simulation. Interested readers could refer to [28,21] for more details. With the adaptive time strategy, larger time steps could be used in the SAV scheme without concerns on stability.

3.2. Full discretization scheme

At each time step, the scheme (31) leads to a linear coupled PDEs for (ϕ^{n+1}, μ^{n+1}) which is essentially a tenth-order PDE for ϕ^{n+1} . This PDE can be easily solved in the case of periodic boundary conditions in all directions. However, we have to deal with one non-periodic direction here, which leads to, for each Fourier mode, a tenth-order PDE in the x -direction with non-periodic direction. This can be efficiently and accurately by using a spectral-Galerkin method with generalized Jacobi polynomials [12,33]. We now describe below our spatial discretization.

We are actually approximating the function space A given in (19). In the y - z direction, the function has already been expressed in Fourier series, so we just truncate according to the indices \mathbf{k} . Let us define $|\mathbf{k}| = \max\{k_j\}$. The truncation is made by $|\mathbf{k}| \leq N_1$. Thus, we only need to consider the approximation in the x -direction for $\phi_{\mathbf{k}}^n(x)$ and $\mu_{\mathbf{k}}^n(x)$. A finite dimensional function space, which is dependent on the boundary conditions is needed. Because we impose Dirichlet boundary conditions on $\phi_{\mathbf{k}}^n(x)$ and Neumann boundary conditions on $\mu_{\mathbf{k}}^n(x)$, we need two different function spaces. In particular, we use polynomials to form the approximation function spaces.

Let P_N be the space of polynomials of degree less than or equal to N . We define two finite dimensional polynomial spaces by

$$W_N = \text{span}\{\varphi \in P_N : \frac{\partial^j}{\partial x^j} \varphi(-L) = \frac{\partial^j}{\partial x^j} \varphi(L) = 0, j = 0, 1, 2, 3\}, \tag{35}$$

and

$$V_N = \text{span}\{h \in P_N : \frac{\partial}{\partial x} h(-L) = \frac{\partial}{\partial x} h(L) = 0\}. \tag{36}$$

We now describe how to deal with the boundary condition (14). Using the form (19), we deduce that

$$\frac{d^j}{dx^j} \phi_s^R(\pm L, \tilde{\mathbf{r}}) = \sum_{\mathbf{k} \in \mathbb{Z}^d} \frac{d^j}{dx^j} \phi_{s\mathbf{k}}^R(\pm L) \exp(\mathbf{i}\mathbf{k}^t \tilde{\mathbf{B}}^t \tilde{\mathbf{r}}), j = 0, 1, 2, 3, \tag{37}$$

where we recall that $\phi_{s\mathbf{k}}^R(x)$ is calculated by (24). Hence, for each \mathbf{k} , we can construct a polynomial $\phi_{0\mathbf{k}}(x) \in P_7$ such that

$$\frac{d^j}{dx^j} \phi_{0\mathbf{k}}(-L) = \frac{d^j}{dx^j} \phi_{1\mathbf{k}_1}^R(-L), \frac{d^j}{dx^j} \phi_{0\mathbf{k}}(L) = \frac{d^j}{dx^j} \phi_{2\mathbf{k}_2}^R(L), j = 0, 1, 2, 3. \tag{38}$$

Then, for each \mathbf{k} , we look for approximation of $\phi_{\mathbf{k}}(x) \in W_{N\mathbf{k}}$ with

$$W_{N\mathbf{k}} = \{f(x) = h(x) + \phi_{0\mathbf{k}}(x) : h(x) \in W_N\}. \tag{39}$$

Hence, at the $(n + 1)$ -th time step, we look for $\phi_N^{n+1}(x, \tilde{\mathbf{r}})$ and $\mu_N^{n+1}(x, \tilde{\mathbf{r}})$, the approximation of ϕ and μ at t_{n+1} , in the following form:

$$\phi_N^{n+1}(x, \tilde{\mathbf{r}}) = \sum_{|\mathbf{k}| \leq N_1} \phi_{N\mathbf{k}}^{n+1}(x) \exp(\mathbf{i}\mathbf{k}^t \tilde{\mathbf{B}}^t \tilde{\mathbf{r}}) \quad \text{with} \quad \phi_{N\mathbf{k}}^{n+1} \in W_{N\mathbf{k}}, \tag{40}$$

and

$$\mu_N^{n+1}(x, \tilde{\mathbf{r}}) = \sum_{|\mathbf{k}| \leq N_1} \mu_{N\mathbf{k}}^{n+1}(x) \exp(\mathbf{i}\mathbf{k}^t \tilde{\mathbf{B}}^t \tilde{\mathbf{r}}) \quad \text{with} \quad \mu_{N\mathbf{k}}^{n+1} \in V_N, \tag{41}$$

which satisfy the following boundary conditions:

$$\frac{\partial^j}{\partial x^j} \phi_N^{n+1}(-L, \tilde{\mathbf{r}}) = \Pi_{N_1} \frac{\partial^j}{\partial x^j} \phi_1^R(-L, \tilde{\mathbf{r}}), \frac{\partial^j}{\partial x^j} \phi_N^{n+1}(L, \tilde{\mathbf{r}}) = \Pi_{N_1} \frac{\partial^j}{\partial x^j} \phi_2^R(L, \tilde{\mathbf{r}}), j = 0, 1, 2, 3, \tag{42}$$

where Π_{N_1} is the Fourier projection operator in the $\tilde{\mathbf{r}} = (y, z)$ directions, and

$$\frac{\partial}{\partial x} \mu_N^{n+1}(\pm L, \tilde{\mathbf{r}}) = 0. \tag{43}$$

The fully discretized scheme of (31) is stated as follows: Given ϕ_N^n and μ_N^n , find ϕ_N^{n+1} in the form (40) and μ_N^{n+1} in the form (41), such that for any $v_N(x) \in V_N$, $w_N(x) \in W_N$, and $|\mathbf{k}| \leq N_1$, they satisfy

$$\begin{aligned} & \left(\frac{\phi_N^{n+1} - \phi_N^n}{\Delta t}, v_N(x) \exp(-\mathbf{i}\mathbf{k}^t \tilde{\mathbf{B}}^t \tilde{\mathbf{r}}) \right) = - \left(\nabla \mu_N^{n+1}, \nabla v_N(x) \exp(-\mathbf{i}\mathbf{k}^t \tilde{\mathbf{B}}^t \tilde{\mathbf{r}}) \right), \\ & \left(\mu_N^{n+1}, w_N(x) \exp(-\mathbf{i}\mathbf{k}^t \tilde{\mathbf{B}}^t \tilde{\mathbf{r}}) \right) = \\ & c \left((\Delta + 1)(\Delta + q^2) \phi_N^{n+1}, (\Delta + 1)(\Delta + q^2) w_N(x) \exp(-\mathbf{i}\mathbf{k}^t \tilde{\mathbf{B}}^t \tilde{\mathbf{r}}) \right) \\ & + \beta \left(\phi_N^{n+1}, w_N(x) \exp(-\mathbf{i}\mathbf{k}^t \tilde{\mathbf{B}}^t \tilde{\mathbf{r}}) \right) + \frac{r^{n+1}}{\sqrt{E_1[\phi_N^n]}} \left\langle F'(\phi_N^n), w_N(x) \exp(-\mathbf{i}\mathbf{k}^t \tilde{\mathbf{B}}^t \tilde{\mathbf{r}}) \right\rangle \\ & \frac{r^{n+1} - r^n}{\Delta t} = \left\langle \frac{F'(\phi_N^n)}{2\sqrt{E_1[\phi_N^n]}}, \frac{\phi_N^{n+1} - \phi_N^n}{\Delta t} \right\rangle. \end{aligned} \tag{44}$$

In the above, the notation $\langle \cdot, \cdot \rangle$ is a numerical integration to approximate the inner product (\cdot, \cdot) and is bilinear, i.e.

$$\begin{aligned} \langle \lambda_1 a_1(\mathbf{r}) + \lambda_2 a_2(\mathbf{r}), b(\mathbf{r}) \rangle &= \lambda_1 \langle a_1(\mathbf{r}), b(\mathbf{r}) \rangle + \lambda_2 \langle a_2(\mathbf{r}), b(\mathbf{r}) \rangle, \\ \langle a(\mathbf{r}), \lambda_1 b_1(\mathbf{r}) + \lambda_2 b_2(\mathbf{r}) \rangle &= \lambda_1 \langle a(\mathbf{r}), b_1(\mathbf{r}) \rangle + \lambda_2 \langle a(\mathbf{r}), b_2(\mathbf{r}) \rangle. \end{aligned} \tag{45}$$

The approximate inner product $\langle \cdot, \cdot \rangle$ will be specified later in Sec. 3.5.

Theorem 2. The fully discrete scheme (44) admits a unique solution, and is unconditionally energy stable in the sense that

$$\tilde{E}[\phi_N^{n+1}, r^{n+1}] - \tilde{E}[\phi_N^n, r^n] \leq -(\nabla \mu_N^{n+1}, \nabla \mu_N^{n+1}) \leq 0, \quad \forall n \geq 0, \tag{46}$$

where

$$\tilde{E}[\phi_N^n, r^n] = \frac{c}{2}((\Delta + 1)(\Delta + q^2)\phi_N^n, (\Delta + 1)(\Delta + q^2)\phi_N^n) + \frac{\beta}{2}(\phi_N^n, \phi_N^n) + |r^n|^2. \tag{47}$$

Proof. By choosing $v_N = \mu_{N,-\mathbf{k}}^{n+1}$, $w_N = \phi_{N,-\mathbf{k}}^{n+1} - \phi_{N,-\mathbf{k}}^n$ in (44) and summing up over \mathbf{k} , followed by multiplying the last equation of by $2r^{n+1}$, one obtains immediately (46).

Since the scheme (44) is linear, and $\tilde{E}[\phi_N^n, r^n]$ implies $\phi_N^n = 0$ and $r^n = 0$, we conclude that the scheme (44) admits a unique solution. \square

Next, we discuss some implementation details for the scheme (44).

3.3. Solving the linear system

Define an operator

$$\sigma(\tilde{\mathbf{B}}\mathbf{k}) = (\partial_x^2 - |\tilde{\mathbf{B}}\mathbf{k}|^2 + 1)(\partial_x^2 - |\tilde{\mathbf{B}}\mathbf{k}|^2 + q^2). \tag{48}$$

After some calculations, the scheme (44) can be simplified into

$$\begin{aligned} \left(\frac{\phi_{N\mathbf{k}}^{n+1} - \phi_{N\mathbf{k}}^n}{\Delta t}, v_N \right) &= -(\partial_x \mu_{N\mathbf{k}}^{n+1}, \partial_x v_N) - |\tilde{\mathbf{B}}\mathbf{k}|^2 (\mu_{N\mathbf{k}}^{n+1}, v_N), \\ (\mu_{N\mathbf{k}}^{n+1}, w_N) &= c \left(\sigma(\tilde{\mathbf{B}}\mathbf{k}) \phi_{N\mathbf{k}}^{n+1}, \sigma(\tilde{\mathbf{B}}\mathbf{k}) w_N \right) + \beta (\phi_{N\mathbf{k}}^{n+1}, w_N) \\ &\quad + \frac{r^{n+1}}{\sqrt{E_1[\phi_N^n]}} \left\langle F'(\phi_N^n), w_N(x) \exp(-i\mathbf{k}^t \tilde{\mathbf{B}}^t \tilde{\mathbf{r}}) \right\rangle, \\ \frac{r^{n+1} - r^n}{\Delta t} &= \left\langle \frac{F'(\phi_N^n)}{2\sqrt{E_1[\phi_N^n]}}, \frac{\phi_{N\mathbf{k}}^{n+1} - \phi_{N\mathbf{k}}^n}{\Delta t} \right\rangle, \end{aligned} \tag{49}$$

where $\phi_{N\mathbf{k}}^n \in W_N + \phi_{0\mathbf{k}}$, $\mu_{N\mathbf{k}}^n \in V_N$.

Looking at (49), we notice that for different \mathbf{k} , the equation is only coupled by the scalar r^{n+1} . We could decouple the equations for different \mathbf{k} as described below. Let $\varphi_j(x)$ and $h_j(x)$ be a basis of W_N and V_N , respectively. We expand $\phi_{N\mathbf{k}}^n(x)$ and $\mu_{N\mathbf{k}}^n(x)$ by the basis,

$$\phi_{N\mathbf{k}}^n(x) = \sum_j \tilde{\phi}_{j\mathbf{k}}^n \varphi_j(x), \tag{50}$$

$$\mu_{N\mathbf{k}}^n(x) = \sum_j \tilde{\mu}_{j\mathbf{k}}^n h_j(x). \tag{51}$$

Define the vectors $y_{\mathbf{k}}^n = (\tilde{\phi}_{j\mathbf{k}}^n, \tilde{\mu}_{j\mathbf{k}}^n)$, $y^n = (y_{\mathbf{k}}^n)$, and the matrices

$$(S_{1\mathbf{k}})_{j_1 j_2} = c \left(\sigma(\tilde{\mathbf{B}}\mathbf{k}) \varphi_{j_1}, \sigma(\tilde{\mathbf{B}}\mathbf{k}) \varphi_{j_2} \right) + \beta (\varphi_{j_1}, \varphi_{j_2}), \tag{52}$$

$$(S_{2\mathbf{k}})_{j_1 j_2} = (\partial_x h_{j_1}, \partial_x h_{j_2}) + |\tilde{\mathbf{B}}\mathbf{k}|^2 (h_{j_1}, h_{j_2}), \tag{53}$$

$$(S_{3\mathbf{k}})_{j_1 j_2} = (h_{j_1}, \varphi_{j_2}). \tag{54}$$

Then, (49) can be written in the form

$$\begin{pmatrix} S & * \\ * & a \end{pmatrix} \begin{pmatrix} y^{n+1} \\ r^{n+1} \end{pmatrix} = b^n, \tag{55}$$

where a is a constant, the stars occupy one column or one row, and the matrix S is block diagonal,

$$S = \text{diag}(S_{\mathbf{k}}), \quad S_{\mathbf{k}} = \begin{pmatrix} S_{1\mathbf{k}} & -S_{3\mathbf{k}}^t \\ \frac{1}{\Delta t} S_{3\mathbf{k}} & S_{2\mathbf{k}} \end{pmatrix}. \tag{56}$$

Therefore, to solve (55), we could apply the block Gauss elimination by solving the equation of the form $Sy = b$ twice. We mention here that for the simple semi-implicit scheme, it needs to solve $Sy = b$ once for each time step, but stability is

not guaranteed. The SAV scheme pays the price of doubling the computation at each time step for the unconditional energy stability.

Note that the entries of the matrix S are invariant for each time step n , so that they can be precomputed. Next, we shall describe in detail the discretization in the x -direction, and how to form and invert S_k efficiently.

3.4. Discretization in the x -direction

We describe how to construct the function spaces V_N and W_N , for which we make use of the Jacobi polynomials and generalized Jacobi polynomials $\{J_k^{\alpha,\beta}(x)\}$ whose essential properties are summarized in the Appendix.

For the sake of simplicity, we shall assume $L = 1$ in the discussion below.

3.4.1. Basis functions for V_N and W_N

The polynomials in V_N satisfy the boundary conditions (36). As in [31], we construct the basis of V_N , $h_k(x)$, as the linear combination of Legendre polynomials $L_k(x) = J_k^{0,0}(x)$,

$$h_k(x) := L_k(x) - \frac{k(k+1)}{(k+2)(k+3)}L_{k+2}(x), \tag{57}$$

for $k = 0, \dots, N - 2$.

By (77), the generalized Jacobi polynomial (GJP) $J_k^{-4,-4}(x)$ satisfies the homogeneous boundary conditions (35). Hence, we can set the basis functions of W_N to be

$$\varphi_l(x) := J_{l+8}^{-4,-4}(x), \quad l = 0, \dots, N - 8. \tag{58}$$

3.4.2. Computation of the matrix elements in S_k

We have specified the basis $\{\varphi_j(x)\}$ and $\{h_j(x)\}$ above. Now $\phi_{Nk}^n(x)$ and $\mu_{Nk}^n(x)$ in (51) can be written as

$$\phi_{Nk}^n(x) = \sum_{j=0}^{N-8} \bar{\phi}_{jk}^n \varphi_j(x) = \sum_{j=0}^{N-8} \bar{\phi}_{jk}^n J_{j+7}^{-4,-4}(x), \tag{59}$$

$$\mu_{Nk}^n(x) = \sum_{j=0}^{N-2} \bar{\mu}_{jk}^n h_j(x). \tag{60}$$

We need to assemble the matrix S_k in (56), defined in (52)–(54). It can be done by using the properties given in the Appendix. We describe $(S_{1k})_{j_1 j_2}$ as an example. The matrix elements contain the terms $(\partial_x^m J_{j_1+7}^{-4,-4}(x), \partial_x^m J_{j_2+7}^{-4,-4}(x))$ where $m = 0, 1, 2, 3, 4$.

- When $m = 4$, the property can be used directly,

$$(\partial_x^4 J_{j_1+7}^{-4,-4}(x), \partial_x^4 J_{j_2+7}^{-4,-4}(x)) \stackrel{(78)}{=} c_1 (J_{j_1+3}^{0,0}(x), J_{j_2+3}^{0,0}(x)) \stackrel{(65)}{=} c_1 \delta_{j_1 j_2},$$

where c_1 is some constant. Only when $j_1 = j_2$ can the term be nonzero.

- When $m = 3$,

$$\begin{aligned} (\partial_x^3 J_{j_1+7}^{-4,-4}(x), \partial_x^3 J_{j_2+7}^{-4,-4}(x)) &\stackrel{(78)}{=} c_2 (J_{j_1+4}^{-1,-1}(x), J_{j_2+4}^{-1,-1}(x)) \\ &\stackrel{(73)}{=} c_2 ((1+x)(1-x) J_{j_1+4}^{1,1}(x), (1+x)(1-x) J_{j_2+4}^{1,1}(x)) \\ &\stackrel{(72)}{=} (c_2^{(0)} J_{j_1+4}^{0,0} + c_2^{(1)} J_{j_1+5}^{0,0} + c_2^{(2)} J_{j_1+6}^{0,0}, c_2^{(0)} J_{j_2+4}^{0,0} + c_2^{(1)} J_{j_2+5}^{0,0} + c_2^{(2)} J_{j_2+6}^{0,0}), \end{aligned} \tag{61}$$

for some constants $c_2, c_2^{(0)}, c_2^{(1)}, c_2^{(2)}$. The term is nonzero only when $|j_1 - j_2| \leq 2$.

- Similarly, we can calculate $(\partial_x^m J_{j_1+7}^{-4,-4}(x), \partial_x^m J_{j_2+7}^{-4,-4}(x))$ for $m = 2, 1, 0$. The term is nonzero only when $|j_1 - j_2| \leq 8 - 2m$.

We could draw the conclusion that S_{1k} is a sparse matrix with at most 17 sub-diagonals. Similarly, S_{2k} and S_{3k} are sparse matrices with at most 5 and 11 sub-diagonals respectively. Moreover, these matrices can be pre-computed with exact analytical expressions.

When solving the linear equation with the coefficient matrix $S_{\mathbf{k}}$, we can precompute and store its LU factorization, because the size of $S_{\mathbf{k}}$ is $2N \times 2N$ that is moderate and $S_{\mathbf{k}}$ are invariant for each time step.

3.5. Numerical integration

We notice that in the scheme (49), we need to compute a numerical integration of the form $\langle F'(u), v \rangle$. Here, the two functions $u(\mathbf{r})$ and $v(\mathbf{r})$ are given in the form

$$u(\mathbf{r}) = \sum_{|\mathbf{k}| \leq N_1} u_{\mathbf{k}}(x) \exp(i\mathbf{k}^t \tilde{B}^t \tilde{\mathbf{r}}).$$

Furthermore, we notice that F' is a third-order polynomial. Thus, we focus on computing the highest-order term $\langle u^3, v \rangle$, and the two lower-order terms can be dealt with in the same way. Since u and v are polynomials of degree less than or equal to N , we find that $u^3 v$ is a polynomial of degree less than or equal to $4N$, which can be exactly integrated if we use Legendre Gauss quadrature of degree $2N$ which is exact for all polynomials of degree less than or equal to $2(2N + 1)$, i.e.,

$$\begin{aligned} \langle u^3, v \rangle &= \frac{1}{2L} \sum_{\mathbf{k}_1 + \mathbf{k}_2 + \mathbf{k}_3 + \mathbf{k}_4 = \mathbf{0}_{[-L, L]}} \int u_{\mathbf{k}_1}(x) u_{\mathbf{k}_2}(x) u_{\mathbf{k}_3}(x) v_{\mathbf{k}_4}(x) dx \\ &= \frac{1}{2L} \sum_{j=1}^{2N} \omega_j \sum_{\mathbf{k}_1 + \mathbf{k}_2 + \mathbf{k}_3 + \mathbf{k}_4 = \mathbf{0}} u_{\mathbf{k}_1}(x_j) u_{\mathbf{k}_2}(x_j) u_{\mathbf{k}_3}(x_j) v_{\mathbf{k}_4}(x_j), \end{aligned} \tag{62}$$

where (x_j, ω_j) are the Legendre Gauss points and weights. Note that the summation about \mathbf{k} can be computed by using FFT in $O((N_1 \log N_1)^d)$ operations.

3.6. Outline of the numerical method

For the computation of quasiperiodic interfacial structure, we list the outline of implementation:

- Find the bulk phase profile in the form (3) by minimizing the free energy density (2). Impose the desired rotation and displacement by (13), from which the boundary conditions and the initial state come from.
- Find the $2 \times d$ matrix \tilde{B} , column full-rank on \mathbb{Q} , for the function space A in (19) consisting of Fourier series. Set the boundary conditions (up to third-order derivatives) and initial state using (24)–(26).
- Discretize the gradient flow (11)–(12) in time using the SAV approach. We apply an unconditional energy stable first-order scheme in order to reach the steady state quickly.
- Discretize in space using spectral method. In the y - z plane, noting that the space A is given by Fourier series, we could simply do the truncation. In the x -direction, we use generalized Jacobi polynomials in accordance with the boundary conditions, which are convenient when dealing with high order derivatives and generate sparse coefficient matrix.
- Different Fourier modes in y - z can be decoupled under SAV. Moreover, the only term that involves different modes is the polynomial term. For quasiperiodic functions, this term can be calculated efficiently by higher dimensional FFT. Although the computational cost is twice as many as the simple semi-implicit scheme at each time step, the SAV enjoys unconditional stability that the semi-implicit scheme does not have.

We must emphasize here that all our derivation depends on that \tilde{B} is column full-rank on \mathbb{Q} . Moreover, the integer d , the number of columns of \tilde{B} , gives the actual dimension of the system, which is $d + 1$ and could be larger than the physical dimension. Thus, the size of discretized system turns out to be $O(N_1^d N)$. Since \tilde{B} depends on the rotations of the two phases, it implies that under different phases or relative orientations, the computational cost will be different. We will illustrate by concrete examples how to choose the matrix \tilde{B} in the next section.

4. Numerical examples

We will consider the three phases introduced above: striped, hexagonal, dodecagonal phases. Their B -matrices are given in (8)–(10). Note that the third row of B is zero for all the three phases. So, the three phases can all be placed in the x - y plane and homogeneous in z -direction. When doing the rotation, we also constrain in the x - y plane, i.e. the rotation matrix T is given by

$$T(\theta) = \begin{pmatrix} \cos \theta & -\sin \theta & 0 \\ \sin \theta & \cos \theta & 0 \\ 0 & 0 & 1 \end{pmatrix}. \tag{63}$$

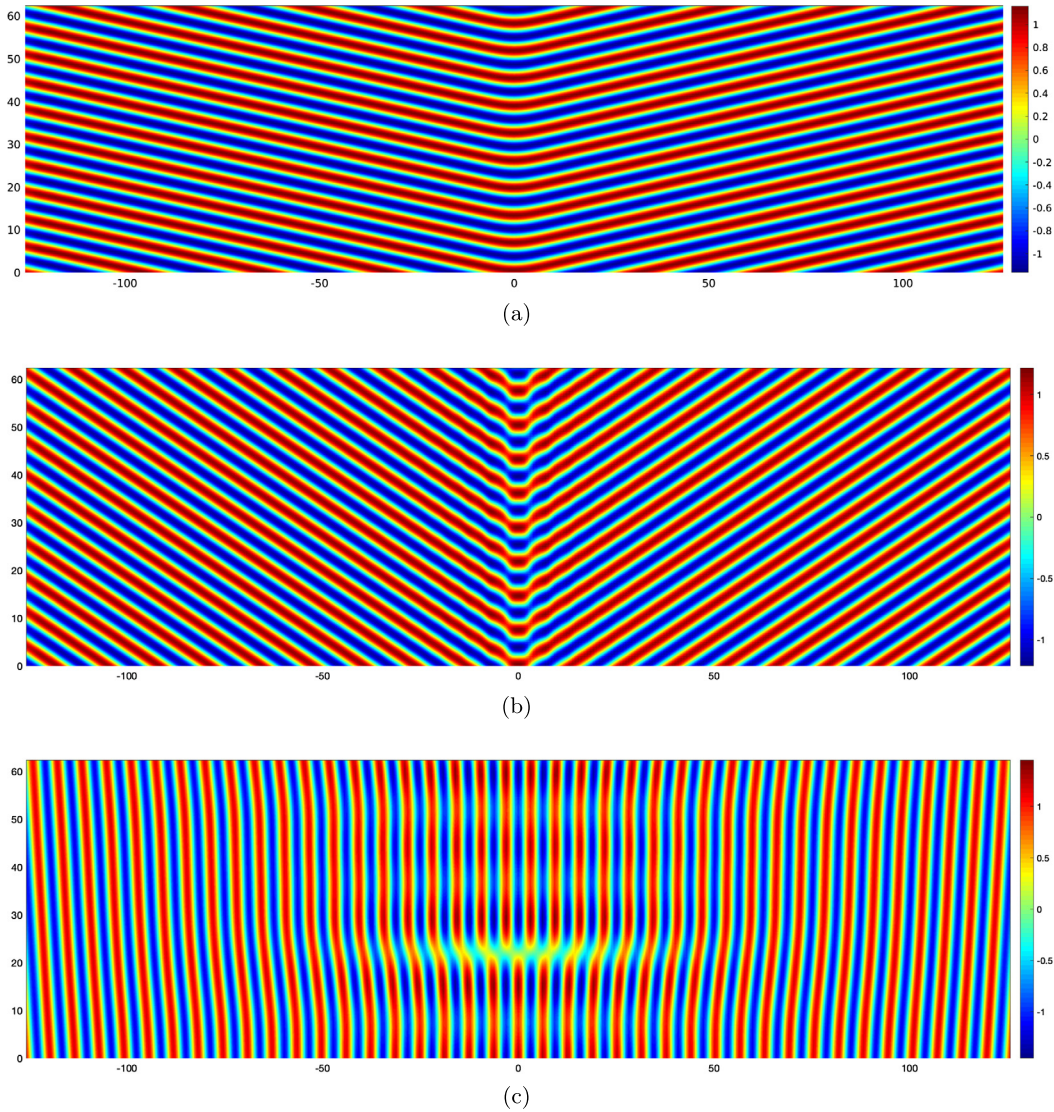


Fig. 3. Profiles of symmetric tilted grain boundaries of striped phase. (a) $\theta = 0.2$; (b) $\theta = 0.5$, (c) $\theta = 1.5$.

As a result, in the interface system, only the first row of the two-row matrix \tilde{B} is nonzero. When determining the column rank of \tilde{B} on \mathbb{Q} , we are actually determining the number of linearly independent real numbers on \mathbb{Q} .

For the parameters in the free energy, we fix the wavelength selecting parameter as $q = 2 \cos(\pi/12)$ and let others vary in order to obtain different phases. In the numerical scheme, the size of spatial discretization in the x -direction is fixed at $N = 256$, and $2N = 512$ Gauss points are used in the numerical integration. The length of the computational domain, L , and the truncation of Fourier series, N_1 , will be suitably chosen for each specific cases. The parameters in the SAV scheme are fixed with $\beta = 4$ and $C_0 = 100$.

4.1. Grain boundaries of striped phase

The phrase ‘grain boundary’ means the interface between two identical phases with different orientations. The grain boundary of striped phases have been studied extensively. Thus, we start from some grain boundaries as a verification of our numerical method.

We examine the tilted grain boundaries of the striped phases. That is, the phase 1 and phase 2 are both the striped phases of the same type with the first B in (8). The phase 1 is rotated by $T_1 = T(\theta)$, while the phase 2 is rotated by $T_2 = T(-\theta)$. Recall that we define $\tilde{B}_1 = \tilde{T}_1^t B$ where \tilde{T}_1 is the second and third columns of T_1 . In this case, we calculate that

$$\tilde{B}_1 = \tilde{T}_1^t B = \begin{pmatrix} \cos \theta \\ 0 \end{pmatrix}, \quad \tilde{B}_2 = \tilde{T}_2^t B = \begin{pmatrix} \cos \theta \\ 0 \end{pmatrix}.$$

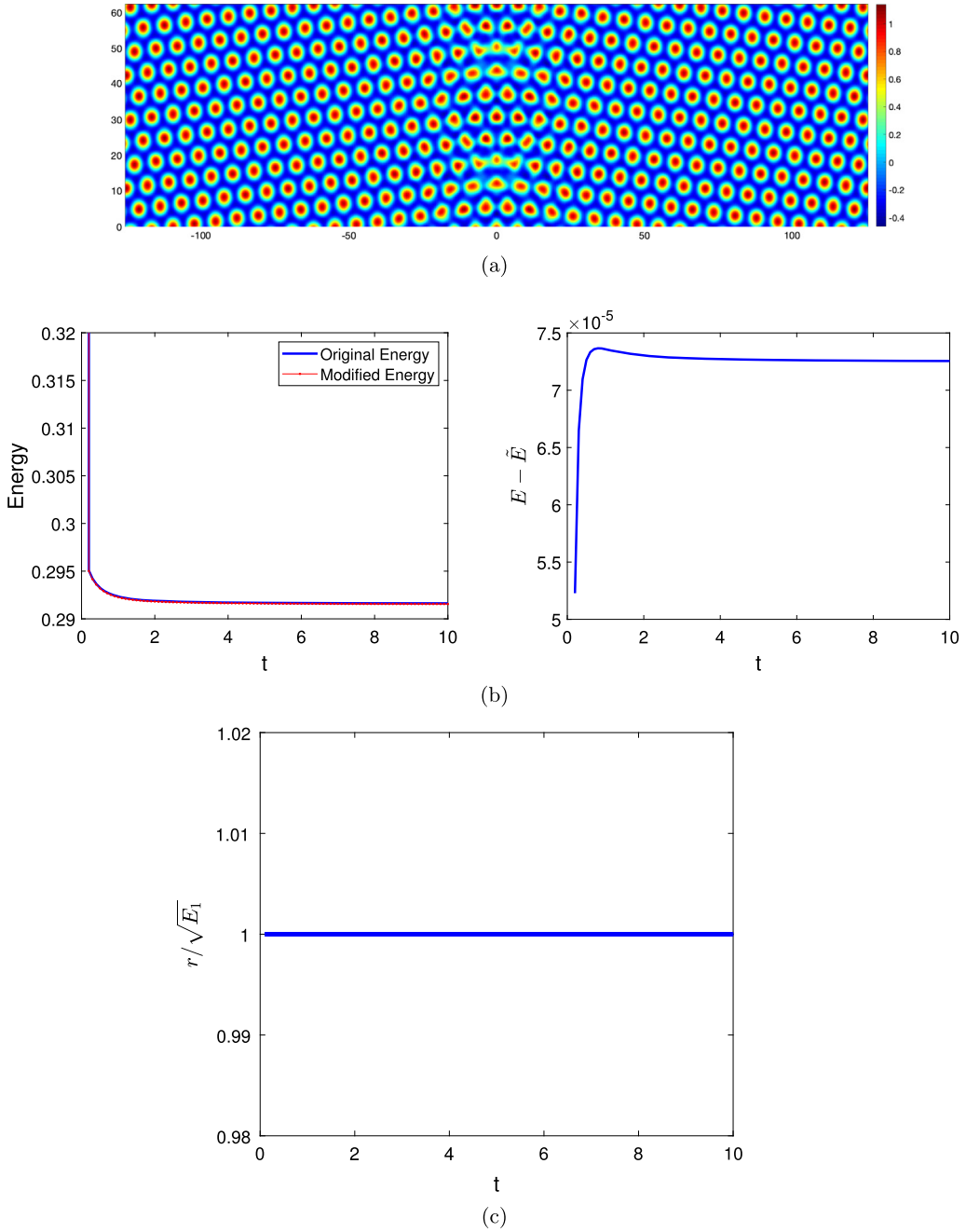


Fig. 4. (a) Profile of symmetric tilted grain boundaries of hexagonal phase with $\theta = \arctan \frac{\sqrt{3}}{4}$. (b) Energy evolution until $t = 10$. (c) Ratio of r to $\sqrt{E_1}$.

Therefore, the \tilde{B} matrix can just be chosen as

$$\tilde{B} = \begin{pmatrix} \cos \theta \\ 0 \end{pmatrix}.$$

It implies that we are actually considering a periodic boundary condition in the y -direction, which is the special case discussed in [41].

We choose $c = 1$, $\alpha = 0$, $\epsilon = 1$, $L = 40\pi$ and $N_1 = 16$. Three different θ 's are considered, for which the steady state can all be reached at $t = 5000$. They are shown in Fig. 3. When θ is small, a smooth transition layer will form; for a larger θ we observe the Omega-shaped patterns in the interface; when θ is near $\pi/2$, a dislocation emerges. These patterns are identical to the previous studies using different free energy [26,23,39].

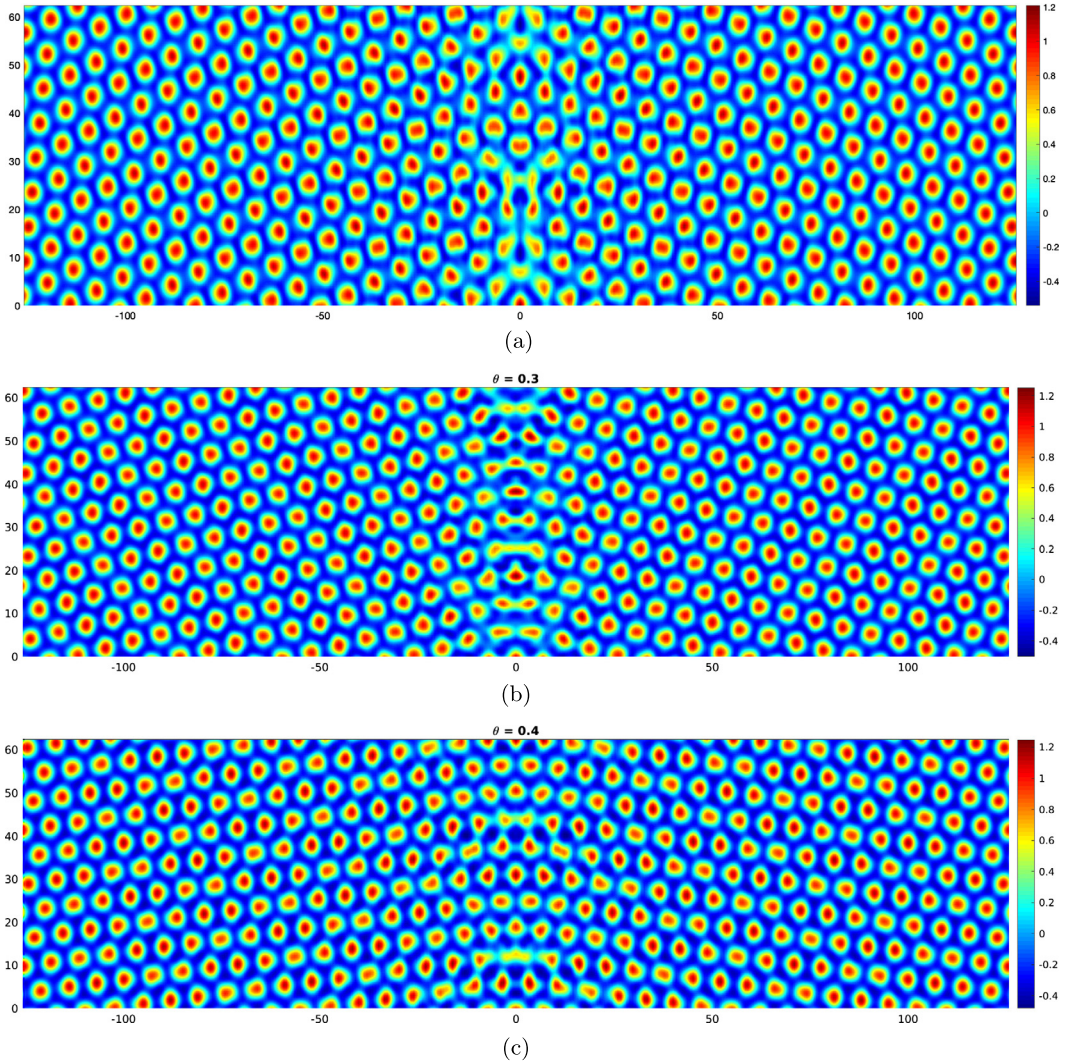


Fig. 5. Profiles for symmetric tilted grain boundaries of hexagonal phase. (a) $\theta = 0.17$; (b) $\theta = 0.3$; (c) $\theta = 0.4$.

4.2. Grain boundaries of the hexagonal phase

We turn to the grain boundaries of the hexagonal phase. We still consider the tilted grain boundaries, letting $T_1 = T(\theta)$ and $T_2 = T(-\theta)$. The case is different from the striped phase, because we may have \tilde{B} of different columns. Let us explain it below.

The B matrix for the hexagonal phase is given as the first one in (9). So, we can calculate that

$$\tilde{B}_1 = \tilde{T}_1^t B = \begin{pmatrix} -\sin \theta & \frac{-\sin \theta + \sqrt{3} \cos \theta}{2} \\ 0 & 0 \end{pmatrix}, \quad \tilde{B}_2 = \tilde{T}_2^t B = \begin{pmatrix} \sin \theta & \frac{\sin \theta + \sqrt{3} \cos \theta}{2} \\ 0 & 0 \end{pmatrix}.$$

If $\tan \theta / \sqrt{3} = m_1 / m_2$ is a rational number, \tilde{B} would have the column rank 1 and can be chosen as

$$\tilde{B} = \begin{pmatrix} \frac{1}{2m_1} \sin \theta \\ 0 \end{pmatrix}.$$

If $\tan \theta / \sqrt{3}$ is not a rational number, then \tilde{B} has the column rank 2 with

$$\tilde{B} = \begin{pmatrix} \frac{1}{2} \sin \theta & \frac{\sqrt{3}}{2} \cos \theta \\ 0 & 0 \end{pmatrix}.$$

We present results for both cases, with the parameters $c = 1, \alpha = 1, \epsilon = 0.15, L = 40\pi$ and $N_1 = 16$. In Fig. 4, we present the grain boundary for $\theta = \arctan \frac{\sqrt{3}}{4}$, the energy dissipation curve, and the ratio $r/\sqrt{E_1}$, where we find that the original

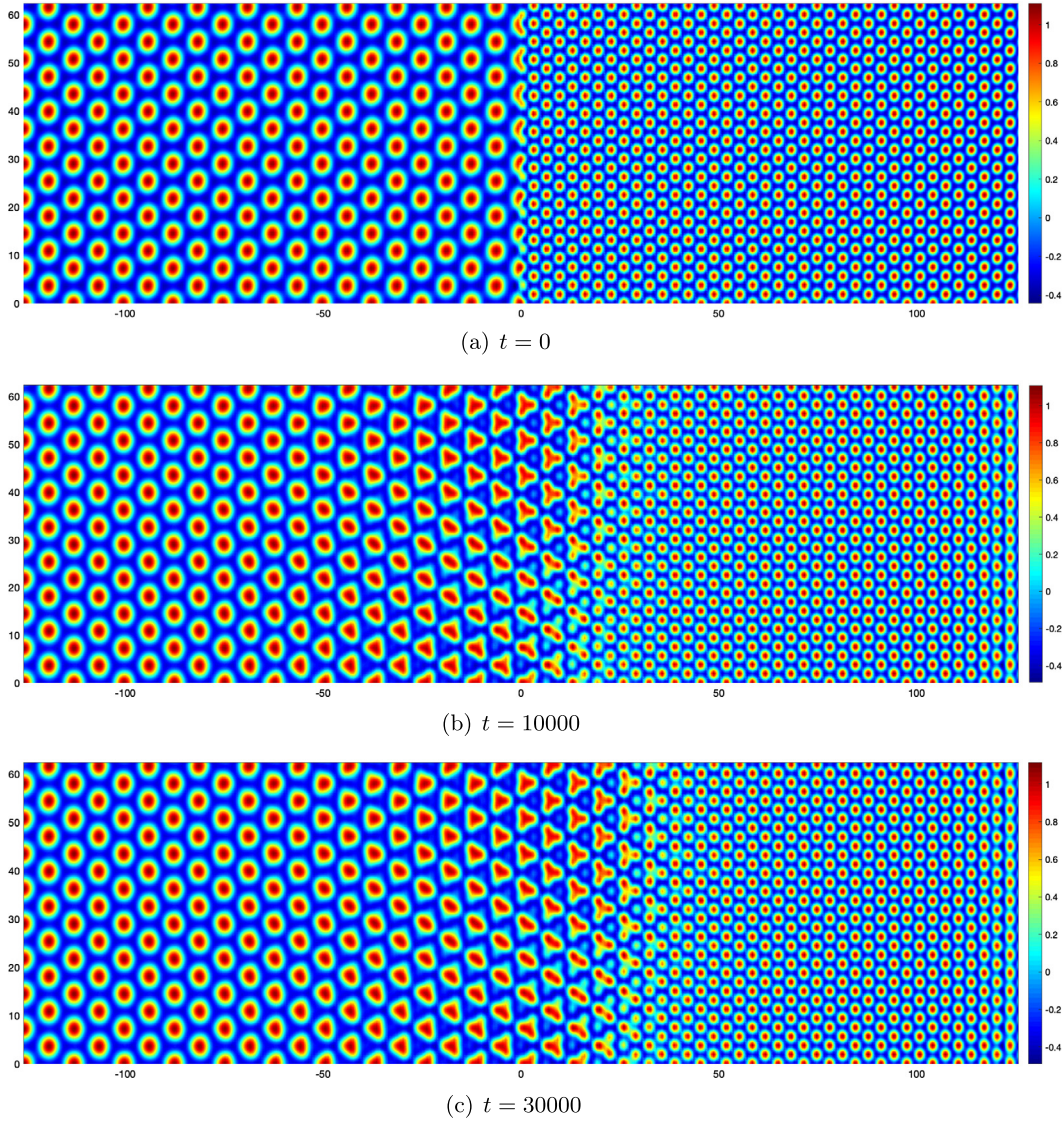


Fig. 6. The evolution of interface between hexagonal phases of different sizes. (a) $t = 0$, (b) $t = 10000$, (c) $t = 30000$.

and modified energy are very close. Then three examples are given in Fig. 5 where $\tan \theta / \sqrt{3}$ is not a rational number. It can be observed that when $\theta = \arctan \frac{\sqrt{3}}{4}$, the hexagonal structures are maintained if more than three circles away from the middle. In contrast, for the three other angles, more connections between the circles are found, and distortion of circles is noticed even far away from the middle.

4.3. Interface between different types of hexagonal phases

Our next simulation is to study the interface between hexagonal phases of different sizes, corresponding to the two B matrices with $|\mathbf{b}_j| = 1$ and $|\mathbf{b}_j| = q$, respectively, given in (9). In this case, we do not impose rotation, so that \tilde{B}_1 and \tilde{B}_2 are just the second and third rows, written as

$$\tilde{B}_1 = \begin{pmatrix} 0 & \frac{\sqrt{3}}{2} \\ 0 & 0 \end{pmatrix}, \quad \tilde{B}_2 = \begin{pmatrix} 0 & \frac{\sqrt{3}}{2}q \\ 0 & 0 \end{pmatrix}.$$

Because $q = 2 \cos(\pi/12)$ is irrational, \tilde{B} can be chosen as

$$\tilde{B} = \begin{pmatrix} \frac{\sqrt{3}}{2} & \frac{\sqrt{3}}{2}q \\ 0 & 0 \end{pmatrix}.$$

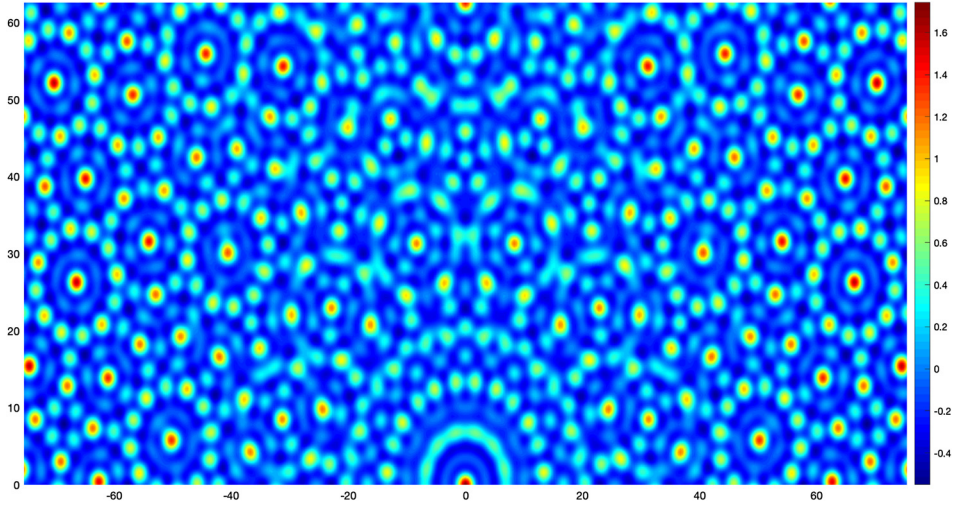


Fig. 7. Profile of the symmetric tilted grain boundary of dodecagonal phase with $\theta = \arctan \frac{\sqrt{3}}{4}$.

The parameters are chosen as $c = 1, \alpha = 1, \epsilon = 0.015, L = 40\pi$ and $N_1 = 16$. The simulation result is presented in Fig. 6, where we show three snapshots. In the initial state, the connection between two hexagonal structures only occurs in the middle. As the time increases, the transition region becomes wider. Many large circles become triangular-shaped, and they gradually rupture into three small ones. Finally, the whole transition region grows to a width of up to ten large circles.

4.4. Grain boundaries of the dodecagonal phase

We simulate the tilted grain boundaries of the dodecagonal phase, letting $T_1 = T(\theta)$ and $T_2 = T(-\theta)$. The matrix B is given in (10) and we have

$$\tilde{B}_1 = \begin{pmatrix} -\sin \theta & -\frac{\sqrt{3}}{2} \sin \theta + \frac{1}{2} \cos \theta & -\frac{1}{2} \sin \theta + \frac{\sqrt{3}}{2} \cos \theta & \cos \theta \\ 0 & 0 & 0 & 0 \end{pmatrix},$$

and

$$\tilde{B}_2 = \begin{pmatrix} \sin \theta & \frac{\sqrt{3}}{2} \sin \theta + \frac{1}{2} \cos \theta & \frac{1}{2} \sin \theta + \frac{\sqrt{3}}{2} \cos \theta & \cos \theta \\ 0 & 0 & 0 & 0 \end{pmatrix}.$$

Therefore, the eight scalars in the first row of \tilde{B}_1 and \tilde{B}_2 can be expressed linearly with rational coefficients by the following four scalars.

$$\frac{1}{2} \sin \theta, \frac{\sqrt{3}}{2} \sin \theta, \frac{1}{2} \cos \theta, \frac{\sqrt{3}}{2} \cos \theta.$$

Thus, for most cases, the column rank of \tilde{B} could be 4. In special cases where either $\tan \theta / \sqrt{3}$ or $\tan \theta$ is rational, the column rank of \tilde{B} is reduced to 2. We here present numerical result of the case with $\theta = \arctan \frac{\sqrt{3}}{4}$. The parameters are chosen as $c = 150, \alpha = 1, \epsilon = 0.015, L = 24\pi$ and $N_1 = 32$. The equilibrium profile is shown in Fig. 7, where we observe a seemingly 24-fold like structure to connect two dodecagonal structures in different orientations.

4.5. Interface between the dodecagonal phase and the hexagonal phase

Our last example is constructed by combining a dodecagonal phase with a hexagonal phase.

$$\tilde{B}_1 = \begin{pmatrix} 0 & \frac{\sqrt{3}}{2} \\ 0 & 0 \end{pmatrix}, \quad \tilde{B}_2 = \begin{pmatrix} 0 & \frac{1}{2} & \frac{\sqrt{3}}{2} & 1 \\ 0 & 0 & 0 & 0 \end{pmatrix}, \tag{64}$$

and \tilde{B} can be chosen as

$$\tilde{B} = \begin{pmatrix} \frac{\sqrt{3}}{2} & \frac{1}{2} \\ 0 & 0 \end{pmatrix}.$$

We choose $c = 1, \epsilon = 0.00833, \alpha = 0.5, L = 24\pi$, and $N_1 = 20$. The equilibrium state and energy dissipation (including original and modified energy, and the ratio $r/\sqrt{E_1}$) are shown in Fig. 8. From the hexagonal region to the dodecagonal region, we find that the circles gradually split and are fitted into the positions of dodecagonal.

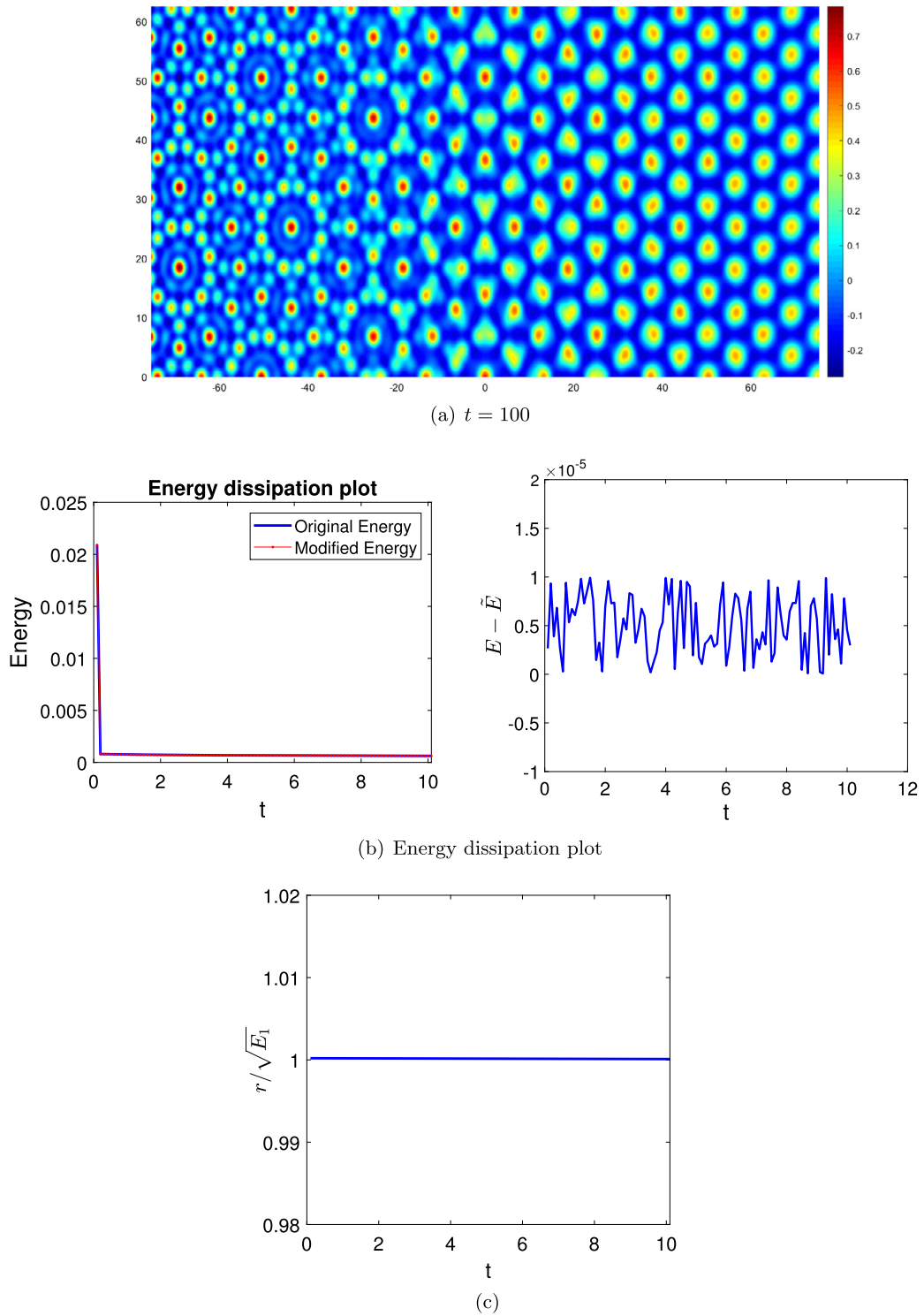


Fig. 8. (a) Profile of the dodecagonal-hexagonal interface. (b) Energy evolution until $t = 10$. (c) Ratio of r to $\sqrt{E_1}$.

5. Conclusion

We proposed a method for computing the interface between two ordered phases that involves quasiperiodicity. With properly chosen function space and boundary conditions to fix the relative orientation and displacement, we solve the H^{-1} gradient flow of the Lifschitz-Petrich free energy, to let the interface evolve to its optimal structure. The gradient flow is

discretized in time by the SAV approach, and in space by a spectral method with a combination of quasiperiodic Fourier series and spectral-Galerkin method using generalized Jacobi polynomials.

We presented numerical simulations using the proposed method for some typical cases, including the interface of the striped, hexagonal and dodecagonal phases. In particular, we show that our numerical method can successfully capture the interfacial structure in the cases where the interface is quasiperiodic.

Thanks to its efficiency and accuracy, the method proposed in this work will allow us to perform systematic simulations of the interface between ordered structures. In a future work, we aim to utilize the method to investigate interface involving other phases, especially the three-dimensional phases, including the bcc/fcc spherical and gyroid that are periodic, and icosahedral quasicrystals.

CRediT authorship contribution statement

Duo Cao: Investigation, Software, Visualization, Writing - original draft. **Jie Shen:** Funding acquisition, Methodology, Writing - review & editing. **Jie Xu:** Conceptualization, Funding acquisition, Methodology, Writing - original draft, Writing - review & editing.

Declaration of competing interest

The authors declare that they have no known competing financial interests or personal relationships that could have appeared to influence the work reported in this paper.

Appendix A. Jacobi polynomials and generalized Jacobi polynomials

We first recall the classical Jacobi polynomials and their properties (cf. [33]). For $\alpha, \beta > -1$, let $J_n^{\alpha, \beta}$ be the classical Jacobi polynomials that are orthogonal with respect to the weight function $\omega^{\alpha, \beta}(x) = (1-x)^\alpha(1+x)^\beta$ over $(-1, 1)$, i.e.

$$\int_{-1}^1 J_n^{\alpha, \beta}(x) J_m^{\alpha, \beta}(x) \omega^{\alpha, \beta}(x) dx = \gamma_n^{\alpha, \beta} \delta_{mn}, \tag{65}$$

where

$$\gamma_n^{\alpha, \beta} = \|J_n^{\alpha, \beta}\|_{\omega^{\alpha, \beta}(x)}^2 = \frac{2^{\alpha+\beta+1} \Gamma(n+\alpha+1) \Gamma(n+\beta+1)}{(2n+\alpha+\beta+1)n! \Gamma(n+\alpha+\beta+1)}, \tag{66}$$

and δ_{mn} is the Dirac delta symbol. Jacobi polynomials have the following properties.

Property 1. Three-term recurrence relationship:

$$\begin{aligned} J_{n+1}^{\alpha, \beta}(x) &= (a_n^{\alpha, \beta} x - b_n^{\alpha, \beta}) J_n^{\alpha, \beta}(x) - c_n^{\alpha, \beta} J_{n-1}^{\alpha, \beta}(x), \quad n \geq 1, \\ J_0^{\alpha, \beta}(x) &= 1, \quad J_1^{\alpha, \beta}(x) = \frac{1}{2}(\alpha + \beta + 2)x + \frac{1}{2}(\alpha - \beta), \end{aligned} \tag{67}$$

where

$$\begin{aligned} a_n^{\alpha, \beta} &= \frac{(2n + \alpha + \beta + 1)(2n + \alpha + \beta + 2)}{2(n + 1)(n + \alpha + \beta + 1)}, \\ b_n^{\alpha, \beta} &= \frac{(\beta^2 - \alpha^2)(2n + \alpha + \beta + 1)}{2(n + 1)(n + \alpha + \beta + 1)(2n + \alpha + \beta)}, \\ c_n^{\alpha, \beta} &= \frac{(n + \alpha)(n + \beta)(2n + \alpha + \beta + 2)}{(n + 1)(n + \alpha + \beta + 1)(2n + \alpha + \beta)}. \end{aligned} \tag{68}$$

The relationship effectively defines the Jacobi polynomials, and enables us to compute their values at any given point $x \in [-1, 1]$.

Property 2. Derivative relationship:

$$\partial_x^k J_n^{\alpha, \beta}(x) = d_{n,k}^{\alpha, \beta} J_{n-k}^{\alpha+k, \beta+k}(x), \quad n \geq k, \tag{69}$$

where

$$d_{n,k}^{\alpha, \beta} = \frac{\Gamma(n+k+\alpha+\beta+1)}{2^k \Gamma(n+\alpha+\beta+1)}. \tag{70}$$

The next property is useful in the computation of the elements in matrix S_k .

Property 3. The Jacobi polynomials satisfy

$$J_n^{\alpha+1,\beta} = \frac{2}{2n + \alpha + \beta + 2} \frac{(n + \alpha + 1)J_n^{\alpha,\beta} - (n + 1)J_{n+1}^{\alpha,\beta}}{1 - x}, \tag{71}$$

$$J_n^{\alpha,\beta+1} = \frac{2}{2n + \alpha + \beta + 2} \frac{(n + \beta + 1)J_n^{\alpha,\beta} + (n + 1)J_{n+1}^{\alpha,\beta}}{1 + x}. \tag{72}$$

We then recall the generalized Jacobi polynomials (GJP) introduced in [11]:

$$J_n^{k,l}(x) = \begin{cases} (1-x)^{-k}(1+x)^{-l}J_{n-n_0}^{-k,-l}(x) & \text{if } k, l \leq -1 \\ (1-x)^{-k}J_{n-n_0}^{-k,l}(x) & \text{if } k \leq -1, l > -1 \\ (1+x)^{-l}J_{n-n_0}^{k,-l}(x) & \text{if } k > -1, l \leq -1 \end{cases} \tag{73}$$

where $n \geq n_0$, $n_0 = -(k+l)$, $-k, -l$ for the above 3 cases respectively and $J_{n-n_0}^{k,l}$ is classical Jacobi polynomial with $k, l \geq -1$. We now present some basic properties of GJP:

Property 4. The GJPs are mutually orthogonal with respect to the generalized Jacobi weight $\omega^{k,l}(x) = (1-x)^k(1+x)^l$, i.e.,

$$\int_{-1}^1 J_n^{k,l}(x)J_m^{k,l}(x)\omega^{k,l}(x)dx = \gamma_{n-n_0}^{\bar{k},\bar{l}} \delta_{mn}, \tag{74}$$

where $\gamma_{n-n_0}^{\bar{k},\bar{l}}$ is defined in (66) and

$$\bar{k} = \begin{cases} -k, & k \leq -1 \\ k, & k > -1 \end{cases} \tag{75}$$

Some GJPs satisfy the homogeneous Dirichlet boundary conditions, making them useful for discretizing PDE.

Property 5. If $k, l \in \mathbb{Z}$ and $k, l \geq 1$

$$\partial_x^i J_n^{-k,-l}(1) = 0, \quad i = 0, 1, \dots, k - 1; \tag{76}$$

$$\partial_x^j J_n^{-k,-l}(-1) = 0, \quad j = 0, 1, \dots, l - 1. \tag{77}$$

The GJPs satisfy derivative relations similar to Property (70).

Property 6. Let $k, l, m \in \mathbb{N}$, and if $m \leq k, l$ then

$$\partial_x^m J_n^{-k,-l}(x) = (-2)^m \frac{(n-k-l+m)!}{(n-k-l)!} J_{n-m}^{-k+m,-l+m}(x), \quad n \geq \max(k+l, m). \tag{78}$$

Using above properties, GJP and their derivatives can be computed recursively.

References

- [1] Andrew J. Archer, A.M. Rucklidge, Edgar Knobloch, Quasicrystalline order and a crystal-liquid state in a soft-core fluid, *Phys. Rev. Lett.* 111 (16) (2013) 165501.
- [2] Kobi Barkan, Michael Engel, Ron Lifshitz, Controlled self-assembly of periodic and aperiodic cluster crystals, *Phys. Rev. Lett.* 113 (9) (2014) 098304.
- [3] S.A. Brazovskii, Phase transition of an isotropic system to a nonuniform state, *Sov. Phys. JETP* 41 (1) (1975) 85–89.
- [4] Lizhen Chen, Direct solver for the Cahn-Hilliard equation by Legendre-Galerkin spectral method, *J. Comput. Appl. Math.* 358 (2019) 34–45.
- [5] Qing Cheng, Jie Shen, Xiaofeng Yang, Highly efficient and accurate numerical schemes for the epitaxial thin film growth models by using the SAV approach, *J. Sci. Comput.* 78 (3) (2019) 1467–1487.
- [6] P.G. De Gennes, J. Prost, *The Physics of Liquid Crystals*, 2nd edition, Oxford Science Publications, Clarendon Press/Oxford University Press, Oxford/New York, 1993.
- [7] Tomonari Dotera, Mean-field theory of Archimedean and quasicrystalline tilings, *Philos. Mag.* 87 (18) (2007) 3011–3019.
- [8] K.R. Elder, Martin Grant, Modeling elastic and plastic deformations in nonequilibrium processing using phase field crystals, *Phys. Rev. E* 70 (5) (2004) 051605.
- [9] Glenn H. Fredrickson, *The Equilibrium Theory of Inhomogeneous Polymers*, Clarendon Press, 2006.

- [10] Glenn H. Fredrickson, Eugene Helfand, Fluctuation effects in the theory of microphase separation in block copolymers, *J. Chem. Phys.* 87 (1) (1987) 697–705.
- [11] Benyu Guo, Jie Shen, Lilian Wang, Optimal spectral–Galerkin methods using generalized Jacobi polynomials, *J. Sci. Comput.* 27 (1) (2006) 305–322.
- [12] Benyu Guo, Jie Shen, Lilian Wang, Generalized Jacobi polynomials/functions and their applications, *Appl. Numer. Math.* 59 (5) (2009) 1011–1028.
- [13] Kenichi Hayashida, Tomonari Dotera, Atsushi Takano, Yushu Matsushita, Polymeric quasicrystal: mesoscopic quasicrystalline tiling in abc star polymers, *Phys. Rev. Lett.* 98 (19) (2007) 195502.
- [14] Weizhang Huang, David M. Sloan, The pseudospectral method for third-order differential equations, *SIAM J. Numer. Anal.* 29 (6) (1992) 1626–1647.
- [15] Kai Jiang, Wei Si, High-order energy stable schemes of incommensurate phase-field crystal model, *Electron. Res. Arch.* 28 (2020) 1077.
- [16] Kai Jiang, Jiajun Tong, Pingwen Zhang, Anchang Shi, Stability of two-dimensional soft quasicrystals in systems with two length scales, *Phys. Rev. E* 92 (4) (2015) 042159.
- [17] Kai Jiang, Pingwen Zhang, Numerical methods for quasicrystals, *J. Comput. Phys.* 256 (2014) 428–440.
- [18] Kai Jiang, Pingwen Zhang, Anchang Shi, Stability of icosahedral quasicrystals in a simple model with two-length scales, *J. Phys. Condens. Matter* 29 (12) (2017) 124003.
- [19] E.I. Kats, V.V. Lebedev, A.R. Muratov, Weak crystallization theory, *Phys. Rep.* 228 (1993) 1–91.
- [20] Andriy V. Kyrylyuk, Johannes G.E.M. Fraaije, Three-dimensional structure and motion of twist grain boundaries in block copolymer melts, *Macromolecules* 38 (20) (2005) 8546–8553.
- [21] Ruo Li, Wenbin Liu, Heping Ma, Moving mesh method with error-estimator-based monitor and its applications to static obstacle problem, *J. Sci. Comput.* 21 (1) (2004) 31–55.
- [22] Ron Lifshitz, Dean M. Petrich, Theoretical model for Faraday waves with multiple-frequency forcing, *Phys. Rev. Lett.* 79 (Aug 1997) 1261–1264.
- [23] M.W. Matsen, Kink grain boundaries in a block copolymer lamellar phase, *J. Chem. Phys.* 107 (19) (1997) 8110–8119.
- [24] N.D. Mermin, Sandra M. Troian, Mean-field theory of quasicrystalline order, *Phys. Rev. Lett.* 54 (14) (1985) 1524–1527.
- [25] Jules Mikhael, Johannes Roth, Laurent Helden, Clemens Bechinger, Archimedean-like tiling on decagonal quasicrystalline surfaces, *Nature* 454 (7203) (2008) 501–504.
- [26] R. Roland Netz, David Andelman, M. Schick, Interfaces of modulated phases, *Phys. Rev. Lett.* 79 (6) (1997) 1058–1061.
- [27] Aldo D. Pezzutti, Daniel A. Vega, Marcelo A. Villar, Dynamics of dislocations in a two-dimensional block copolymer system with hexagonal symmetry, *Philos. Trans. R. Soc., Ser. A* 369 (1935) (2011) 335–350.
- [28] Zhonghua Qiao, Zhengru Zhang, Tao Tang, An adaptive time-stepping strategy for the molecular beam epitaxy models, *SIAM J. Sci. Comput.* 33 (3) (2011) 1395–1414.
- [29] Michael Seul, David Andelman, Domain shapes and patterns: the phenomenology of modulated phases, *Science* 267 (5197) (1995) 476–483.
- [30] D. Shechtman, I. Blech, D. Gratias, John W. Cahn, Metallic phase with long-range orientational order and no translational symmetry, *Phys. Rev. Lett.* 53 (20) (1984) 1951–1953.
- [31] Jie Shen, Efficient spectral–Galerkin method I: direct solvers of second- and fourth-order equations using Legendre polynomials, *SIAM J. Sci. Comput.* 15 (6) (1994) 1489–1505.
- [32] Jie Shen, A new dual–Petrov–Galerkin method for third and higher odd-order differential equations: application to the KDV equation, *SIAM J. Numer. Anal.* 41 (5) (2003) 1595–1619.
- [33] Jie Shen, Tao Tang, Lilian Wang, *Spectral Methods: Algorithms, Analysis and Applications*, vol. 41, Springer Science & Business Media, 2011.
- [34] Jie Shen, Jie Xu, Convergence and error analysis for the scalar auxiliary variable (SAV) schemes to gradient flows, *SIAM J. Numer. Anal.* 56 (5) (2018) 2895–2912.
- [35] Jie Shen, Jie Xu, Jiang Yang, The scalar auxiliary variable (SAV) approach for gradient flows, *J. Comput. Phys.* 353 (2018) 407–416.
- [36] Jie Shen, Jie Xu, Jiang Yang, A new class of efficient and robust energy stable schemes for gradient flows, *SIAM Rev.* 61 (3) (2019) 474–506.
- [37] J. Swift, P.C. Hohenberg, Hydrodynamic fluctuations at the convective instability, *Phys. Rev. A* 15 (Jan 1977) 319–328.
- [38] Roger Temam, *Infinite-Dimensional Dynamical Systems in Mechanics and Physics*, 2nd edition, Springer, 1997.
- [39] Yoav Tsoori, David Andelman, M. Schick, Defects in lamellar diblock copolymers: Chevron- and Ω -shaped tilt boundaries, *Phys. Rev. E* 61 (3) (2000) 2848–2858.
- [40] Xiangfa Wu, Tianyou Fan, Dongmei An, Energy release rate of plane quasicrystals with crack determined by path-independent E-integral, *Chin. J. Comput. Mech.* 17 (1) (2000) 34–42.
- [41] Jie Xu, Chu Wang, An-Chang Shi, Pingwen Zhang, Computing optimal interfacial structure of modulated phases, *Commun. Comput. Phys.* 21 (1) (2017) 1–15.
- [42] L.Z. Yang, F.M. He, Yang Gao, Finite element method for static problems of cubic quasicrystals, *Acta Phys. Pol. A* 126 (2) (2014) 471–473.
- [43] Xiaofeng Yang, Daozhi Han, Linearly first- and second-order, unconditionally energy stable schemes for the phase field crystal model, *J. Comput. Phys.* 330 (2017) 1116–1134.
- [44] Xiaofeng Yang, Lili Ju, Linear and unconditionally energy stable schemes for the binary fluid–surfactant phase field model, *Comput. Methods Appl. Mech. Eng.* 318 (2017) 1005–1029.
- [45] Xiangbing Zeng, Goran Ungar, Yongsong Liu, Virgil Percec, Andres E. Dulcey, Jamie K. Hobbs, Supramolecular dendritic liquid quasicrystals, *Nature* 428 (6979) (2004) 157–160.
- [46] Zhengru Zhang, Yuan Ma, Zhonghua Qiao, An adaptive time-stepping strategy for solving the phase field crystal model, *J. Comput. Phys.* 249 (2013) 204–215.